Needle Insertion Mechanism for Robot Assisted Biopsy

A Major Qualifying Project (MQP) Report
Submitted to the Faculty of
WORCESTER POLYTECHNIC INSTITUTE
in partial fulfillment of the requirements
for the Degree of Bachelor of Science in

Robotics Engineering,

By:

James Doherty

Project Advisors:

Christopher Nycz

Date: March 2024

Abstract

This project aimed to investigate the use of robotic platforms to increase accuracy and improve patient outcomes in ultrasound-guided biopsy procedures. The specific procedure chosen for investigation was percutaneous renal biopsy because it represents an increasing category of in-office guided procedures performed by a single physician. I present the design of an end effector and procedures for using a generic articulated arm to serve as a collaborative guide for a physician to take ultrasound-guided biopsies of the kidneys. Surgical robotics has obvious application to more significant procedures; the advantages of comprehensive imaging and a sedated patient allow for more automated movement, which increases dexterity precision, and ultimately patient outcomes. However, imagery-intensive partially or fully sedated procedures represent only a minority of medical interventions. Through this project, I intended to investigate the potential for robotic assistance in more minor procedures carried out in-office by an individual physician using less comprehensive imaging tools. In the context of more minor procedures, a robot must serve as a minimally disruptive collaborative tool for its user.

The overall system I designed consisted of an end effector mounted on a generic industrial 6DOF articulated arm and an optical tracking system to localize the ultrasound probe. The ultrasound probe is tracked by a single camera mounted in the robot's end effector; an April tag mounted to the probe allows for a transformation matrix to be calculated between the probe and the current position of the robotic arm. Using this transformation along with the kinematics of the robot arm itself, the physician can identify biopsy targets and plan approaches in the 2D image space of the ultrasound probe, and the system can use the inverse kinematic model of the arm to calculate poses and trajectories in the 3d workspace. The robotic arm is a small industrial robot unsuitable for surgical use. I chose the industrial arm due to availability; thus, it lacks many features necessary for collaborative operation. This hardware limitation meant that certain aspects of the system's implementation had to remain theoretical with the ABB industrial arm used. However, the system was designed with the assumption of its hypothetical replacement with an articulated arm more suitable to the application. An external IK and path planning tool is used to calculate safe paths around the workspace, ultimately bringing the robot to a minimum safe distance from the patient from which a physician could safely bring the tool head up to the patient. The end effector is a guide for the needle insertion axis; it is constructed around a set of linear bearings and contains sensors for linear position and on-axis load applied to the biopsy needle. While the actuation of the insertion axis is in the hands of the physician, the axis does implement force control through the use of a pneumatic cylinder with a variable flow rate, the purpose of which is to provide both haptic feedback to the physician and to be able to hold the axis in position if necessary. Overall, this project represents a potential approach for using robotics as a collaborative tool for ultrasound-guided procedures.

Contents

List of Tables

List of Figures

1 Introduction

Percutaneous renal biopsy (PRB) is essential in diagnosing and managing kidney disease. Due to the kidney's nature as a highly vascular organs, the procedure carries an increased risk of hematoma. Using ultrasound guidance enables more precise needle guidance, thus reducing necessary insertions and trauma to the kidney. However, current ultrasound-guided PRB procedures present limited insertion paths or require multiple attending surgeons due to the complexity of operating the ultrasound probe and guiding the biopsy gun. The development of robot-assisted PRB can simplify the procedure's surgical requirements and allow more flexibility in procedure planning, needle path, and operation monitoring.

Medical robotics as a field has naturally tended towards a particular category of procedure: those involving large highly accurate imaging equipment, full or partial patient sedation, requiring multiple or highly skilled medical personnel to perform, and where the existing procedure uses complex or limiting tools from some of the earliest uses of medical robotics in fields such as the Minerva system for CT-guided stereostatic brain biopsy to the increasing clinical use of systems such as the DaVinci platform for minimally invasive procedures in the ventral cavity. Medical robotics is well suited to these applications; high-accuracy imaging, precisely planned operations, and an unmoving, well-modeled work environment lend themselves well to robotic precision. Significant work has been done on a particular model of robotic surgery that places the medical personnel as 'operators' while the robot manipulates the tools. This division of tasks is quite fitting; it would be much more challenging for a surgeon to achieve the dexterity of a DaVinci manipulator using traditional laparoscopic tools or precisely biopsying a specific point on an MRI of the brain.

Renal biopsy does not share the characteristics of 'traditional' robotic surgeries. Ultrasound provides a two-dimensional image highly susceptible to probe location and orientation; the biopsy is performed with just local anesthesia, often by a single interventional radiologist, and using tools no more complex than a biopsy needle and small probe-mounted needle guide. It would be possible to design a surgical robot to perform renal biopsies using a traditional 'surgeon as operator' approach; replace the ultrasound with the much more rarely used MRI, fully sedate the patient, enable the surgeon to plan in full three-dimensional detail of the needle trajectory and final biopsy point, and then let the robot collect the biopsy. This theoretical approach would take biopsies with greater accuracy, enable a wide range of insertion paths, and likely ultimately improve patient outcomes; unfortunately, no doctor would ever use it. The increase in cost and complexity would negate any improvements; a procedure that can be done 'in-office' would now require an anesthesiologist, a surgical prep team, and an operating theater with an MRI. For robotic PRBs to improve patient outcomes, the procedure must improve on existing methods and acknowledge the requirements that

shaped those methods.

A PRB that incorporates the advantages of robotics must remain in the hands of the surgeon, with the robot taking an assistive role. The nature of ultrasound imaging and the challenges of the biopsy are much better addressed by the surgeon's direct control of the instruments used. If the surgeon controls the instruments, the role of any robotic system is assistive; therefore, the robot cannot significantly impede the surgeon's workflow and must increase rather than decrease approaches to the procedure. Any proposed solution will, therefore, draw heavily on the concept of collaborative robotics and work with, not against existing biopsy workflow.

The exploration of robot-assisted renal biopsy has the potential to offer insight into a broader array of more 'minor' procedures in which collaborative or assistive robotics can enable surgeons to enhance current practices to improve patient outcomes.

1.1 Project Objectives

When identifying project objectives I intended to structure the project in such a way as to identify critical knowledge at each step before proceeding, it was my intention to avoid implementing unnecessary or unrealistic features. While no project is ever neatly linear the following tasks were mostly completed in order.

1.1.1 Task 1

Identify a procedure workflow and system architecture that allows physicians to access the increased capabilities of robotic assistance whilst minimizing inconvenience and avoiding introducing new limits to the procedure. This robot is intended to assist with a already existing surgical procedure and as such should be designed with consideration for existing practices.

1.1.2 Task 2

Design and build a manipulator that allows for robotic location and orientation of the biopsy needle while enabling the physician precise control of the movement of the needle itself. Given the physicians attention will likely be focused on the ultrasound image the manipulator should be ergonomically intuitive and capable of some degree of haptic feedback. Sensors should be implemented to allow for accurate location of the needle tip and identify any aberrant loading or potential deflection

1.1.3 Task 3

Design and program the control architecture of the system including ultrasound image to workspace coordinate transformation, path planning and obstacle avoidance, responsive force feedback, and effective GUI.

2 Background

The purpose of a PRB is to collect a sample of material from the kidney for testing. This procedure is crucial to diagnosing kidney disease, with an estimated 58100 performed annually across the US.[5] As with all biopsy procedures, safety and yield are critical to the outcome. In a renal biopsy, yield is measured by the quantity of glomeruli [6], clusters of capillaries around tubules in the kidney, with an optimal number of collected glomeruli for diagnostic purposes being between 10-15, though often 6-10 can prove sufficient [7].

2.1 Biopsy Collection

Historically, renal biopsy was commonly performed with a 15G manually operated core sample biopsy needle. This device comprises a needle and concentric hypotube; the central needle is a solid core and notched along its length. After insertion of the biopsy device, the central needle is extended into the tissue to be sampled, and the external sheath is then slid forward cutting a specimen that is now trapped inside the notched needle.

While manually operated biopsy needles were historically used, modern PRBs typically use a spring-loaded biopsy device. These devices, commonly called 'biopsy guns,' use a preloaded spring to increase the speed and force with which the external sheath collects its sample. Cozens et al. measured an improvement of biopsy success rate to 97% through the use of spring-loaded biopsy needles compared to non-sprung collection methods [8], the quality increase is attributed to the speed of the cut reducing crush artifacts in the collected core. Needles on spring-loaded biopsy guns are often of a smaller gauge with 18G being commonly used, though depending on circumstance anywhere between 14G and 18G needles can be used [9]. Taking a core biopsy is almost always needed for diagnostic purposes. Alternatively, when performing focal renal biopsy (biopsy of specific masses in the kidney typically for diagnosis of potential renal cancers) both core and fine needle samples are taken [9].

Despite the advantages, using these larger automated devices presents some complications as their size and weight often require two hands to use suitably. Consequently, most institutions have two doctors perform the procedure [10], and some use a fixed trajectory needle guide affixed to the ultrasound probe [11].

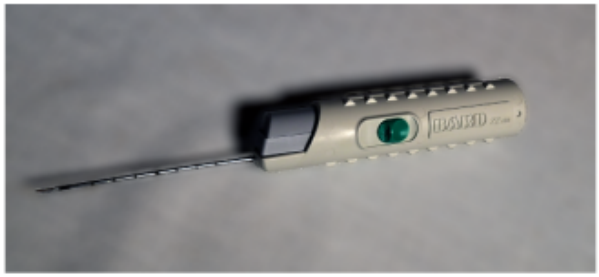

Figure 1: A example of a common 14G spring loaded biopsy needle. (MC1410, Bard, Franklin Lakes, NJ, USA)

2.2 Ultrasound Guidance

Medical ultrasound uses a transducer mounted in a probe to non-invasively image a patient. The imaging is live, producing a 2D slice of the imaged tissue with density represented by image intensity. Unlike more comprehensive imaging methods such as CT or MRI scans, an ultrasound is typically lower resolution and, due to the free movement of imaged tissue and probe, challenging to relate to 3D imaging. The comparative strength of ultrasound is that it is a simpler and cheaper procedure that allows for easy live monitoring of an operation.

When performing a PRB guided by ultrasound, the needle is typically inserted 'in plane' with the ultrasound probe so that its entire length is visible in the ultrasound image. Figure 2 contains an example of a typical insertion, the needle being visible as a bright line. When performing a guided biopsy, best practice often calls for moving the probe independently of the needle to allow the surgeon to understand the needle's position relative to the kidney and other obstructions.

Ultrasound-guided percutaneous renal biopsy is a procedure that uses the ultrasound probe to allow a physician to guide the biopsy needle into the kidney more accurately. The introduction of ultrasound guidance to PRB procedures in the early 2000s saw significant increases in Glomuli collected and decreases in minor and major complications. [10] At the time of introduction, ultrasound-guided percutaneous renal biopsies were exclusively performed by Nephrologists. PRBs typically require two or more attending surgeons, one to operate the ultrasound probe and another to handle the biopsy needle. As the procedure has evolved, a shift has been made to interventional radiologists, who are typically solely responsible for ultrasound operation and needle management.

One of the challenges of ultrasound guidance is keeping the needle in the plane and thus visible to the probe. A solution to this problem can be found in probe-mounted needle guides. These simple mechanical devices can be attached to the edge of ultrasound probes and allow for needle insertions at a

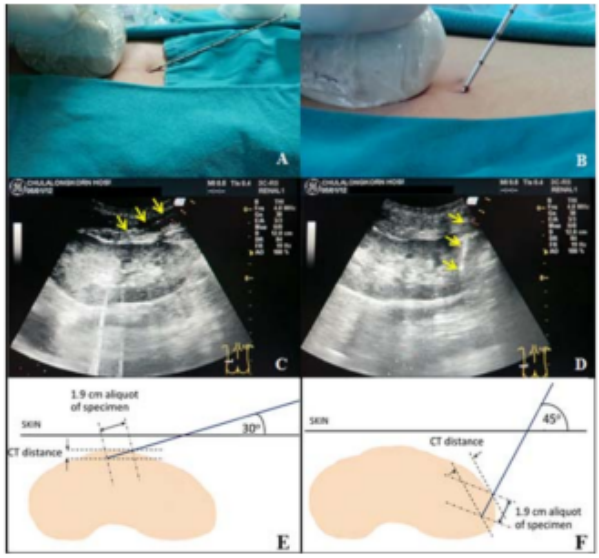

Figure 2: A figure reproduced from Chancharoenthana et al. study of unique kidney biopsy sampling trajectories [1]. This figure combines the ultrasound image visible to the surgeon, the external view of probe and needle, and a diagram of the kidney and intended needle depth. The images in the left hand column represent the unique shallow angle approach being tested, while the right hand column demonstrates a more typical approach.

fixed angle relative to the probe's central axis. Figure 3 contains an example of a common model of one of these manual needle guides. A study released in 2017 observes that the adoption of probe-mounted needle guides resulted in an increase in material collected and a decrease in minor complications. [12] The study also notes that the manual guides enabled the move of renal biopsy to a single-operator procedure. Using needle guides while allowing for reduced surgical staff comes with certain limitations, notably a narrow band of angles easily achievable by the guide and preventing free movement of the probe during insertion.

2.3 Changing Clinical Practice

Renal biopsy as a procedure was typically performed by or under the supervision of nephrologists; however, the increasing trend is for PRBs to be completed by radiologists. The number of PRBs performed by nephrologists fellows has been in steady decline since 1984 [13] though this is not due to decreasing relevance as the procedure has been increasing in frequency over the same timeframe. Instead, PRBs are more commonly performed by interventional radiologists.

While such changes in clinical procedure are generally harmless and reflect the increasing frequency of guided percutaneous biopsy in general, in the case of renal biopsy, the change has coincided with a decrease in successful outcomes. A study by Arkana Laboratories of rates of 'missed' biopsies (procedures in which

Figure 3: A prototypical example of a probe mounted 'manual' needle guide. (Protek^{TM} 1-535-7461, Aspen Surgical, Caledonia, MI, USA)

insufficient glomeruli were collected for diagnosis) demonstrated a general increase in miss rate from 2% to 14% in 2020, with some centers producing a miss rate as high as 50%[14]. The study attributed this increase to the change in operators. The study concluded that as that trend is unlikely to reverse itself, new methods of training or operation are required to increase the success rate when performed by less specialized medical personnel.

The change in operator has also come with an increase in post-operation complications. A study in 2005 found that while Interventional Radiologists did not, on average, take more samples during a biopsy, they saw a significant increase in post-op complications compared to nephrologists.[15]

2.4 Potential benefits of nontraditional needle trajectories

Recent research has indicated some benefits to alternative procedures for percutaneous renal biopsy requiring different geometries of ultrasound probe and biopsy needle relative to the sampled kidney. A study in 2014 achieved significant increases in Glomuruli collected and a slight decrease in hematoma by sampling from the middle of the kidney with an approach angle of approximately 30 degrees.[1] While the paper concludes that this new approach can be adopted surgically without significant change in training, it is worth noting

that the shallower angle is not achievable with the manual US-mounted needle guides.

While the 2014 study was relatively small and does not appear to have been replicated, other studies reveal the significant difference in outcomes caused by relatively minor changes in approach angle and targeted kidney operation. A 2019 study published in the Journal of the Canadian Association of Radiologists found significant increases in glomeruli collected and hematoma rates from changes in approach angle of 20 degrees or less. [16] This study was focused on a narrower range of angles associated with the more traditional high-angle biopsy approach, so it does represent needle trajectories compatible with probe-mounted needle guides. However, the significance of minor angle changes does suggest that there are increases in procedure outcomes to be achieved by providing surgeons with increased capability for procedure planning and finer control of needle trajectory.

2.5 Prior Research

To inform my work on this project, I began with a study of current literature covering the use of robots for biopsies, along with the solutions for integrating ultrasound guidance with robotic systems. I am certainly not the first to identify the potential benefits of robot-performed or assisted biopsies, and many others have done impressive theoretical and practical work on this problem. My work is informed by and builds upon other's approaches, but represents a unique application of current approaches to a specific procedure. This paper will present another approach to the task and expand the corpus of knowledge around this subject.

Robotized biopsy marked the first introduction of robots to the surgical suite in the mid-1980s, performing CT-guided neurosurgery. The first robotized biopsy was completed in 1985 at Memorial Medical Center using a modified industrial arm to achieve and then hold a predetermined orientation as it was used to orientate drills and biopsy probes [17]. Following initial successes, relatively few innovations were made in robotic biopsy: the introduction of MRI guidance [18], and robotic spinal biopsy [19] some of the most notable. The lack of growth in robotic biopsy use beyond applications with extreme precision and rigidity can be attributed to the limitations of contemporary technology. Changing technology and the growth and success of surgical robotics led to rapid innovations in robotized biopsy in the late 2000s and 2010s [20]. A review of existing biopsy robots in the Current Robotics Reports [21] recognizes specific challenges and trends. Most notable is the observation that most work on robotic biopsy focuses on either breast or prostate biopsy, focusing on diagnosing cancers in both organs. Other observations made from the review include the use of high DOF serial chain actuators to increase workspace. Additionally, while some procedures may make the insertion under ultrasound monitoring, most robotized biopsy relies on pre-procedure MRI or CT

scan imaging. A significant observation of robotic biopsy is that while many prototypes use autonomous needle insertion, they are primarily in the prototype or early design stage. In contrast, those designs in clinical trials or surgical use have passive or, at most, semi-active needle control. It is unclear as to the exact reason for this; however, personal conversations with industry-side engineers have suggested surgeon control of needle insertion being necessary to receive regulatory approval. However, without developed standards or guidance from organizations such as the FDA [22], active needle control is not prohibited but likely would require a clear and specific use case.

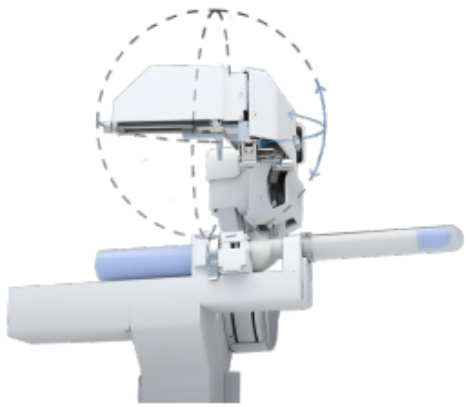

Figure 4: The Mona Lisa Prostate biopsy robot. The upper section is the robotic needle guide responsible for aligning the biopsy needle for surgeon insertion. The lower tube-like section contains the endocavity ultrasound probe. (iSR'obot Mona Lisa, Biobot Surgical, Singapore)

Prostate Biopsy is one of the most explored robotic biopsy procedures due to certain favorable conditions that provide significant potential for robotic intervention, and the high number of procedures performed across the US. A prostate biopsy is traditionally performed with a minimally invasive technique involving the insertion of an ultrasound transducer and biopsy tool through the rectum. A biopsy tool is inserted coaxially to the ultrasound probe and is used systematically to collect a spread of samples with the patient under a local anesthetic [23]. An MRI may be taken of a patient before the biopsy and can be used to identify specific tumors or other sites of interest. In addition to a diagnostic MRI scan, performing the biopsy under MRI guidance is possible to enable alternative transperineal or transgluteal approaches or targeted transrectal biopsy when needed [23]. The circumstances of prostate biopsy are well suited to robotic assistance, the minimal deformation of tissues while probing, and the lack of other organs around or near the insertion paths. The most common robot for prostate biopsy is the MonaLisa platform produced by BioBot Surgical Ltd; the MonaLisa platform, figure 4, uses a pre-operation MRI and transrectal probe manipulated by the robot to construct a live model of the prostate area and align a needle guide with depth stop for transperineal biopsy collection [24]. I would be remiss not to mention the work done at WPI on active

MRI-guided prostate biopsy (figures 5, 6) using needle rotation to correct for observed needle deflections from the planned insertion axis [2]. This thesis paper provided particular inspiration in designing procedure workflow and the potential for needle axis force measurements to identify membrane punctures or areas of differing density, such as cysts or tumors.

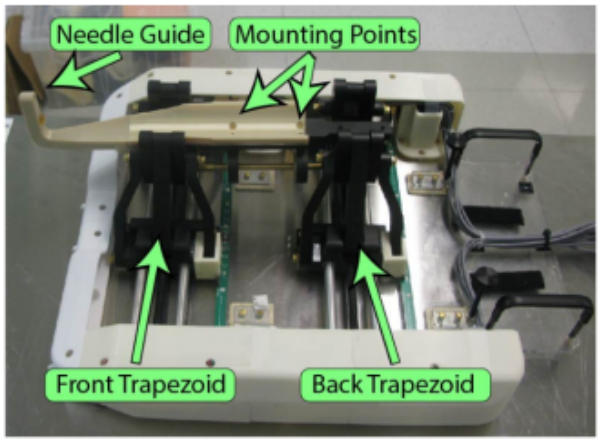

Figure 5: Labelled image of MRI safe prostate biopsy robot reproduced from Wartenberg's thesis [2]. This 4DOF piezo electric motor driven robot was originally developed by Fischer et al. [3]. The robot has an entirely manual needle guide providing only axial alignment without any depth measurement or control.

Though examining prostate biopsy robots is informative, some critical differences from renal biopsy must be understood. The rectal ultrasound probe performs radial scans, meaning that a single-axis linear insertion movement is sufficient to construct an array of 'sliced' ultrasound images; the radial scan, along with limited access, limits active ultrasound procedure monitoring to out-of-plane scans to control insertion depth. The linear ultrasound transducers used for renal biopsy also collect 2D images, but the scanning method involves 6DOF movement both to comply with the shape of the patient and to keep the kidney in the picture; this freedom of probe movement also extends to procedure monitoring with insertions typically performed in-plane with out of plane scans to confirm position and depth. This difference in ultrasound procedure makes it much simpler to control rectal probe movements with a robot than to perform the same controlled scan and MRI matching in a renal procedure.

Breast Biopsy is the other area that has seen the most significant development of robotized biopsies. While breast biopsies can be performed using MRI or mammogram guidance, they are most often performed using simple ultrasound guidance from the same linear or curvilinear ultrasound probe used in Renal biopsies. Ultrasound-guided breast biopsies can be achieved with or without pre-operation MRIs.[25] Much of the research into robotic breast biopsy focuses on MRI-guided procedures and the development of compact MRI-safe robots. The Stormram 3 robot presented in a paper from 2017[26] is an example of this approach. While

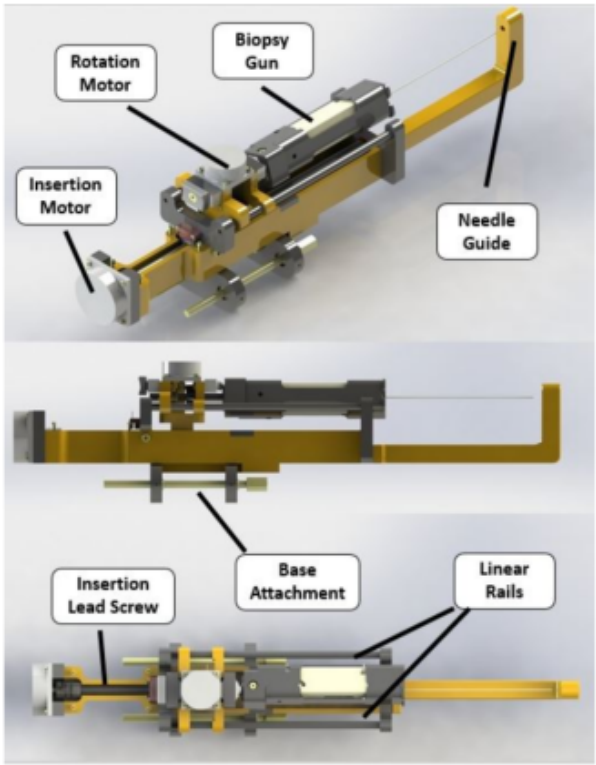

Figure 6: Labelled render of the active needle control manipulator developed by Wartenberg in his thesis [2]. This is an example of a fully active needle guide containing both depth measurement and insertion force detection along with full robotic control of the needle insertion.

the work is impressive, it does not provide much insight into my work, as the complexity of MRI guidance would be impractical for most renal biopsies. The approach outlined by Chen et al. using optical mapping of local tissue to localize an MRI or other pre-operation image to the workspace is of more interest.[27] Though this paper does not present a complete surgical system or workflow, topography matching is notable as it allows the procedure to be performed outside an MRI and with a completely uncoupled ultrasound probe. Some methods for ultrasound-guided breast biopsy have been prototyped with robot control of the US probe by mounting it to a gantry or articulated arm.[28] There are some interesting ideas, such as using the probe to manipulate the breast and bring a tumor in line with a fixed needle,[29] but otherwise, the work done on robot-controlled probe designs lack answers to the problems of conforming the probe to tissue or address how the surgeon is supposed to work with their only exploratory tool mounted to a robotic arm.

Approaching the research from the other direction, an examination of robotic ultrasound systems, significant work has been done on teleoperated ultrasound systems to allow a remote specialist to manipulate a probe and perform an examination where it is impossible to examine a patient in person. The significant challenge in designing teleoperated ultrasound systems is maintaining gentle contact between probe and

tissue and conforming to curving deformable geometry. As such, many early designs were limited to specific areas of anatomy, such as the carotid or central abdomen [30] seen in Figure 7, and 8 respectively. The increasing capabilities for force-sensitive arms present opportunities to address these issues when combined with optical scanning to conform to a surface under teleoperation or even automatically scan an area.[31] One of the most used teleoperated ultrasound platforms is the ESTELE platform produced by Robosoft seen in Figure 9. The ESTELE platform consists of a frame through which an assistant positions the probe and a spherical wrist controlled remotely [32]. The division of labor allows the more complex task of positioning the probe and maintaining pressure to be performed manually while granting the physician the control needed to perform an ultrasound exploration.

Figure 7: Image of early robotic ultrasound system developed by Abolmaesumi et al. for ultrasound scanning of the cartoid artery [4].

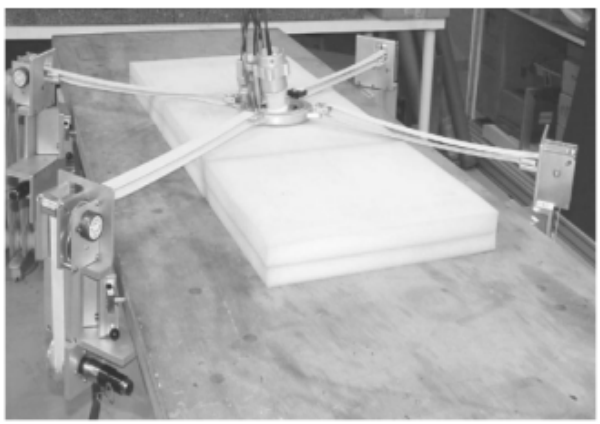

Figure 8: Image of the TER system developed by Vilchis et al. for ultrasound scanning of the abdominal cavity. In operation the robot is held in place over the patients abdomen while the probe is rotated by the robot.

Figure 9: Image of the Estelle teleoperated ultrasound system. (ESTELLE, Robosoft Engineering, Anglet, France) When in use a surgical assistance positions the robot by use of the black frame, while a surgeon can teleoperate the marked degrees of freedom.

The PAKY needle guide developed at Johns Hopkins in 2006 is an early robotic system worth discussing.[33] Though other methods have superseded the x-ray-based "Superimposed Needle Registration," the concepts of operation focusing on collaborative surgeon assistance are still noteworthy. The PAKY system used a passive 7dof arm and an active 2dof wrist. The passive arm was lockable and used to locate the tool over the insertion point with a laser dot for alignment. Once the arm was correctly positioned, the robotic wrist could achieve the correct orientation with a needle guide aligned with the needle target. The design of this system focused on surgeon accessibility and maintaining a simple workflow.

In 2011, a clinical study investigated the use of teleoperated ultrasound in renal biopsy.[34] An ESTELE platform allowed a remote ultrasonographer to examine the kidneys and guide a nephrologist to perform the biopsy. The ultrasound probe was held in place by an assistant or mounted to a passive arm while the biopsy was performed; this allowed the nephrologist to use both hands on the biopsy tools as the ultrasonographer manipulated the probe and provided verbal guidance. This procedure does remove the insertion angle restrictions by separating the responsibility for probe and needle; however, this solution certainly does not increase accuracy. The insertion point was selected using a finger to produce a shadow on the ultrasound, then inserting the tool 'near the finger.' Across the four procedures performed, all samples collected were suitable; however, operation time was increased by 55%, and patient feedback highlighted the inconvenience. Ultimately, while an interesting study, the increased time and complexity, all while requiring more than one physician, suggests that this is not a direction worth further exploration.

3 System Architecture and Workflow

The first step to this project is gathering requirements and making critical decisions regarding system architecture. The selected architecture then informs decisions regarding the procedure workflow. I used weighted objective tables to evaluate potential options to distinguish between significantly different approaches with varying strengths.

3.1 Workspace Definition

Before making architectural decisions, I must define the robot's workspace. I decided to attempt to preserve the existing 'common' layout for renal biopsies for multiple reasons. Primarily, the current placement of patient, surgeon, and ultrasound has been optimized for ease of procedure; in addition, avoiding significant changes to the surgical space fulfills the design requirement of keeping the robot as 'assistant' to the surgeon's procedure. Identifying the 'most common' layout of the surgical area was performed by observing renal biopsies documented for educational purposes primarily accessed through services such as YouTube. Fig 10 represents the layout I identified as most common; the patient is placed face down with the surgeon alongside, and the ultrasound placed within reach of the surgeon towards the patient's head. As renal biopsy is often an in-office procedure, the table used is likely an exam table, meaning the patient's height is fixed. I observed some variation in the placement of tool trays, either over the patient's feet as in the figure or a freestanding tray placed alongside the foot of the bed on the surgeon's side of the patient. Notably, physicians prefer to work on the side of the biopsied kidney, so the doctor will often flip this layout.

From this layout, I defined both the work area and the region where the robot cannot occupy without interfering with the surgeon; these regions are indicated in Fig 11. I defined the workspace of the robot as occupying the width of the exam table, a length equal to about a quarter of the patient's torso, and a height adequate to account for variations in patient size. Within this workspace, the robot should be capable of reaching all needle trajectories greater than 30° from horizontal. The workspace will be centered on the patient's kidneys, thus introducing a need to align the robot with the patient or the patient to the robot; given the identified need to flip the layout, this can be achieved if I mount the system on a wheeled cart. I defined the area the robot cannot occupy as the surgeon's side of the exam table; this is intended not only for safety but also to prevent obstruction of the usual workflow.

Figure 10: Plan view of surgical area

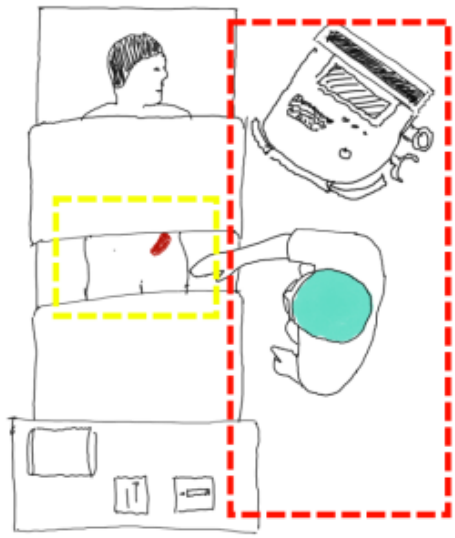

Figure 11: Required work area marked in yellow and keep out zone in red.

	Weight
Obstacle Avoidance	10
Cost	3
Base Stability	5
Safety	3
Manual/Collaborative Operation	5
Existing Medical Usage	8
Volume When Stowed	8

Table 1: Robot Architecture Weights

3.2 Robot Architecture Selection

System architecture selection is critical to overall design considerations as with all robotic applications. I used a weighted objective table considering a series of factors to select between a multiplicity of options with varying costs and benefits. First is the system's overall cost, an element for which there is relatively minimal distinction and is comparatively unimportant. Obstacle avoidance is the capacity to reach the desired end pose configurations while avoiding obstacles in the workspace, ranging from the inconvenient, such as the ultrasound probe and cable, to the critical, like the patient or surgeon. As such, obstacle avoidance is a crucial design consideration, and a higher degree of freedom arm is valued. The size of the robot's base station represents the architecture's stability and overall weight; due to the likely location of the robot base opposite the surgeon, its size and unwieldiness are critical considerations to the effective use of the robotic system. Surgical robotics demands the close interactions of patients and surgeons with the robotic system, so safety is a crucial concern. While many elements of safe design are universal across architectures, some consideration can be made for the amount of weight each architecture puts above the patient and the number of joints whose failure would lead to a robot-patient collision. Collaborative robotics provide many benefits regarding surgeon-robot interactions; as such, I considered how easily each arm could be manually moved, particularly regarding how 'natural' their movement is performing likely manually guided adjustments. I highly rated the existence of surgical robots using that architecture due to the easy availability of 'off the shelf' solutions and because increasing familiarity and comfort with familiar architectures can ease the adoption and use of new technology. The final factor I considered was volume when stowed; this served as a catch-all for the robot's size and ability to clear the work area above the patient to allow easier access. I listed these factors in Table 2 with relative weights corresponding to importance.

The first architecture to consider is an articulated 6 DOF arm (Fig. 12); this robotic solution is common throughout the industry as one of the most efficient and flexible means of achieving a full 6 degrees of freedom. The articulated arm has significant benefits regarding obstacle avoidance as it is technically

Figure 12: Plan view of a articulated arm

over-actuated for the 5 DOF problem. This architecture has a clear advantage in volume when stowed, being able to fold up upon itself for easy stowage and a range of motion that enables it to lift 'away' from the patient in almost any situation. While the additional degree of actuation and associated mass does increase the cost of this system, that disadvantage is made up for by the existence of multiple articulated arms already intended and in use in the surgical context. The commonality of articulated arms makes this architecture appealing; however, it comes with some disadvantages. An articulated arm necessarily incurs the most significant safety risk, suspending a large mass above the patient held by multiple joints. Additionally, the articulated design does not lend itself to intuitive manual operation being quite incomprehensible to jog, and even in a force-controlled collaborative configuration, it can often prove frustrating due to a multiplicity of singularities.

The next architecture follows directly from the rectangular nature of the workspace. A gantry-based arm with actuation in all three cartesian directions and two degrees of orientation at the head (Fig. 13) is likely the cheapest architectural solution as it contains no redundant degrees of freedom or wasted workspace. However, this simplicity comes at a cost as this system would require a much larger base and cannot reduce its volume in a stowed position, resulting in either issues clearing the patient work area or an increased footprint. The defined and unchanging axis of linear motion makes the teleoperation of this type of arm much more intuitive, even if the linear motion often does not reflect natural movements. This architecture has the most minor capability for obstacle avoidance, being both single solution and limited in approach pathing by its need to reach over the patient. There are no current off-the-shelf medical implementations using this architecture.

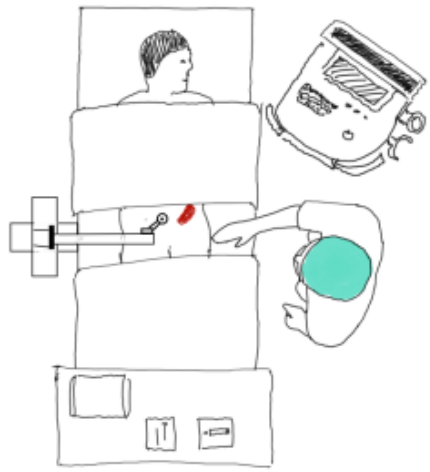

Figure 13: Plan view of a cartesian architecture

A spherical architecture (Fig 14) allows for the cost and weight benefits of a 5 DOF system while addressing some of the concerns regarding stowed volume and base stability. Despite these benefits, it still suffers from having singular inverse kinematic solutions, making obstacle avoidance when achieving a pose and pathing to it much harder. A cylindrical architecture has one significant advantage: it enables much more natural unpowered collaborative operation. By locking out joint 2, the linear z-axis, and letting the other four joints yield, an operator can position the end effector of a spherical robot with relative ease and through much more natural motions compared to the cartesian architecture.

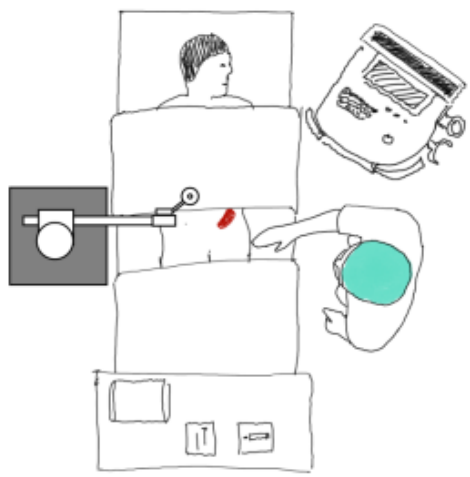

Figure 14: Plan view of a cylindrical architecture

The final architecture worth mentioning is the suspension of a serial or parallel actuator from a

	Articulated	Cartesian	Cylindrical	Suspended
Obstacle Avoidance	4	1	2	3
Cost	2	4	3	1
Base Stability	4	2	3	1
Safety	1	3.5	3.5	2
Manual/Collaborative Operation	1	3	4	2
Existing Medical Usage	3.5	1.5	1.5	3.5
Volume When Stowed	4	1	3	2
Weighted Total	134	77.5	110.5	98

Table 2: Robot Architecture Weighted Objective Table

fixed beam above the patient. While this setup naturally requires a much larger base and likely becomes significantly heavier, the arm can be lighter and slimmer due to the decreased reach. When operating a serial arm in this configuration, you also see improvement in obstacle avoidance, as more binary solutions (elbow inverted) are achievable. For this application, the bulk of the base renders the solution non-viable. It is worth noting however that this architecture is already in use in much larger robots such as Intuitive Surgical's daVinci platform.

When calculating weighted objectives, the articulated architecture emerges as a clear favorite. This result is consistent with the direction and decisions of industry regarding the use of robotic arms for surgical applications.

3.3 Arm Selection

Given the decision to use an articulated arm, the next step was to decide which robotic arm to use. In this case, the most significant deciding factor is if the arm is already used for or intended for medical use. A robotic arm that is designed for medical purposes not only brings end-user familiarity and confidence but also means that the arm is designed with the necessary safety features to allow safe surgical use. In addition to redundant fail-safe brakes and soft-release mechanisms, these arms likely incorporate force-limiting and protected workspace monitoring. These safety considerations are crucial to the robot's approval for actual surgical use. The next most significant factors in arm selection are overall system weight and collaborative functionality. The system weight is important because it directly affects the necessary size and weight of the base cart; minimizing arm weight generates corresponding increases in portability and compactness, enabling the use of the system in more circumstances. Collaborative robotics is an emerging field that will prove crucial to future success in surgical robotics. The precision and rigidity of robotic arms are a welcome addition to any procedure; however, autonomous motion around a patient and surgeon carries significant risk. Surgeons and patients would appreciate the fine positional movement done collaboratively with the

	Weight
Total System Weight	12
Reach	8
Payload Capacity	2
Collaborative	12
Existing Medical Usage	15

Table 3: Robotic Arm Selection Weights

robot adjusting orientation as position changes. Additionally, once the entry position has been achieved, a surgeon may want the ability to make fine adjustments to orientation under their own control. These potential use cases require specific hardware capabilities and design incorporated into the arm to make them possible. Another significant factor in arm choice is reach; while a reduced reach can be compensated for, and all robots considered have a reasonable work area, a more extensive reach allows for a broader range of potential operation locations without requiring reconfiguration of the robot base or surgical table. The final factor considered is payload capacity, which in this application is a relatively meaningless distinction; the needle guide tool will likely be at most 2kg as to weigh more than that would indicate excessive bulk or inefficient material choice. This factor is even more pronounced when considering draping requirements and that most, if not all, of the needle guide will likely be disposable. Table 3 contains the weights assigned to each factor that I will use to evaluate potential robotic arms.

I selected an array of potential robotic arms meant to represent the possible options available, with a particular focus on articulated arms already used in surgical applications. The first arm I selected is the ABB robotics IRB 120-3; this robotic arm is representative of small industrial arms. The ABB arm lacks collaborative features and is not currently used in surgical applications. The Kuka LBR Med is explicitly intended for collaborative medical applications. The LBR Med has haptic feedback capabilities and redundant safety mechanisms, making it a good fit for surgical applications. Stäbuli Rosa is the name of Stäbuli's surgical robot; though the Rosa platform has fewer collaborative features, it is already in surgical use. The overall platform is quite large, integrating a base cart and controller. The final robotic arm I examined was the Universal Robotics UR5e; the UR5e is a collaborative robot intended for industrial applications. Though the UR5e lacks the medical features of the LBR Med or Rosa, its collaborative abilities are extensive.

Examining Table 4, the Kuka LBR Med would be the ideal platform for this application. Unfortunately, there is one overriding category that I did not include: availability. When working on this MQP I had access to an ABB IRB120 robotic arm; though it is not the ideal arm, it will serve to develop and test my ideas. I addressed the ABB arm's lack of collaborative features by using jogging commands instead of

	ABB IRB120-3/06		Kuka LBR Med 7R800		Stäbuli Rosa		UniversalRobotics UR5e	
Weight	25kg	2	25.5kg	3.5	117kg	1	20.6kg	3.5
Reach	0.56m	1	.8m	2	.85m	4	.85m	3
Payload Capacity	3kg	1	7kg	3	12kg	4	5kg	2
Collabritive		1		3		1		4
Existing Medical Usage		1.5		3		4		1.5
Weighted Total		68.5		145		136		140.5

Table 4: Arm selection weighted objective table

	Weight
Cost	5
Portability	8
Feasability	10
Freedom of Motion	8
Additional Probe Mass	5
Interference w/ Probe Grip	3

Table 5: Ultrasound Localization Weights

manually guiding the arm. Though this solution would not be ideal in a surgical setting, it did suffice for my testing and evaluation of the system.

3.4 Ultrasound Probe Localization

A major architectural decision remains on how the robot will collect data from the ultrasound probe. Unlike other procedures, such as prostate biopsy, a guided PRB uses a linear or curvilinear handheld ultrasound probe. I decided quite early that the ultrasound probe should remain under the direct control of the physician. Keeping the probe under the physician's control is intended to enable ease of adoption by avoiding major changes to the existing procedures. Functionally, the robot needs to be able to sense the ultrasound probe's location and orientation relative to the base frame of the surgical system. An optimal solution to probe localization minimizes the 'impact' on the physician's ability to perform the procedure.

One approach to localizing the ultrasound probe would be to attach it to a robotic manipulator, likely another serial chain arm. This approach would be consistent with the prior use of ultrasound imaging in surgical robotics. Using this solution, it would still be possible for the physician to maintain active control of the probe through the use of collaborative robotics; however, if expending the cost and complexity of using a robotic arm, it would only make sense to integrate some degree of automated ultrasound scanning or search performed by the system. Fully or semi-autonomous ultrasound scanning may be an idea worth pursuing in another context but would likely be an unneeded complexity and a barrier to the adoption of robotic involvement in an otherwise fairly 'routine' if complicated procedure. More practically, the use of

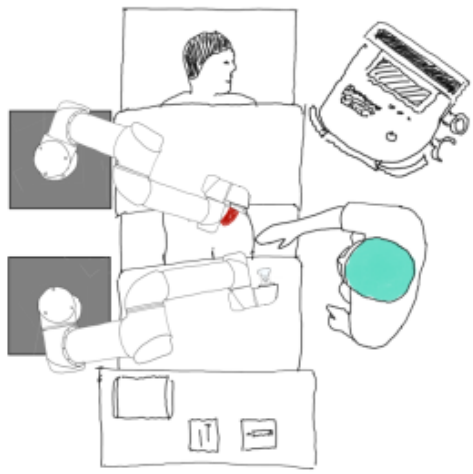

Figure 15: Plan view of fully automated scanning using second arm.

a second serial chain would present serious challenges regarding self-collision and unnecessary cluttering of the operation space.

Another approach to probe localization is to construct a direct mechanical linkage between the needle guide and the ultrasound probe. This linkage would likely be unpowered, yet an accurate positional reference to the ultrasound probe could be acquired by measuring its joints. This approach has the added benefit that the referenced position will be relative to the needle guide itself, thus reducing error accumulation. The mechanical linkage would not need to be large as the distance between the needle guide and probe will remain relatively small during operation. Despite a small size, the mechanical linkage would be complex; the standard use of an ultrasound probe would require six degrees of freedom, both three-dimensional positioning and the unimpeded rotation of the probe for various forms of exploration and scanning. Connecting the probe and needle guide introduces an additional complexity; physicians may find it frustrating to be unable to effectively use the ultrasound probe without the needle guide already in position. In addition, in a surgical context, the ultrasound machine is likely to be used for other procedures, so making a permanent attachment to an ultrasound probe would be counterproductive, limiting the options for mechanical attachment.

When examining the unpowered mechanical linkage in the context of my weighted objective table, I rated it favorably in cost and overall size and weight. The mechanical linkage does not compare favorably with its comparatively limited freedom of movement and the likely interference with the physician's ability to grip and thus use the ultrasound probe. The final and likely disqualifying trait of the mechanical linkage is its complexity and, thus, feasibility. Implementing this method requires an unpowered 6 DOF kinematic chain with a high focus on freedom of orientation pivoting around a set of axes not contained within the system.

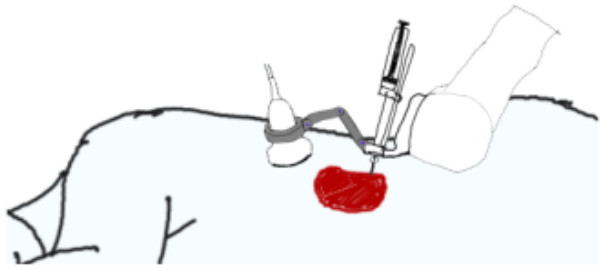

Figure 16: Probe localization by mechanical linkage to needle guide.

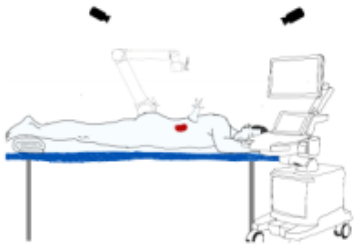

Figure 17: Probe localization by OptiTrack using multiple cameras.

This is not an impossible design problem; however, solving it at a suitably small scale while maintaining the necessary accuracy and ease of use would be a significant challenge.

With the ultrasound probe's mechanical tracking options examined, the next logical option to consider is optical tracking. The most comprehensive form of optical tracking would be using a multi-camera system such as OptiTrack. Using multiple cameras set up and calibrated to cover the intended workspace, any object within that workspace can be tracked using a 'constellation' of markers affixed to the item. A multi-camera tracking system would enable maximum freedom of motion for the probe, as the tool's position and orientation can be calculated so long as the constellation remains visible. An additional constellation placed on the robotic arms base, or even on the needle guide itself, would provide the rest of the necessary frames to enable easy localization of the biopsy target. The major drawbacks of a multicamera system are cost and portability. The need for multiple cameras rigidly placed along with other considerations, such as lighting, make equipping an area for Optitrack usage a complex and expensive task. Surgical theaters could be, and in some cases are, equipped with this level of optical tracking equipment; however, the requirement to perform PRB's 'in office' would make a multi-camera tracking system impractical.

The final option for probe localization was using a single-camera system. Using a singular camera, likely attached to the robotic arm in some manner, the probe can be localized via a flag or other tracking

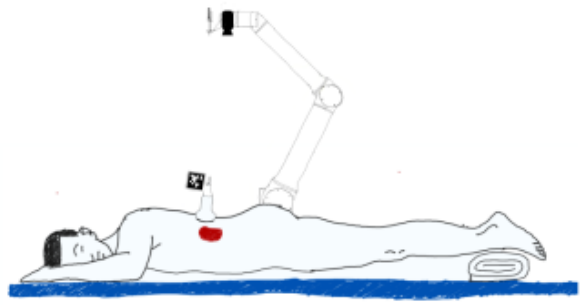

Figure 18: Probe localization by AprilTag using single camera.

	Full Automation	Unpowered Arm	OptiTrack multiple cameras	AprilTag single camera
Cost	1	3	2	4
Portability	1	4	2	3
Feasability	2	1	4	3
Freedom of Motion	1	2	4	3
Additional Probe Mass	NA	1	2.5	2.5
Interference w/ Probe Grip	NA	1	2	3
Weighted Total	41	81	116.5	119.5

Table 6: Ultrasound localization weighted objective table

graphic attached to it. A single-camera system does not offer the full range of motion of a multi-camera system; the limitations of a single-camera field of view combined with the need to keep the tracking graphic visible to the camera will limit the range of positions and orientations the probe can be used in. With careful selection of the camera used, its placement, and careful placement of the tracking graphic, effective coverage can likely be achieved for the relatively small range of positions and orientations used during a PRB. The flags for the tracking graphics are likely to be larger and more unwieldy than a constellation yet can still be positioned so as not to interfere with the probe's normal operation. The most crucial benefit of a single-camera system is portability. By affixing the camera to the robotic arm, the system can be wheeled to a patient's bedside and ready for operation almost immediately. A single camera system would require no external components or preparation beyond a tracking flag affixed to the ultrasound probe. T

Ultimately, I selected the single-camera method for use in this project; though slightly less accurate and more restrictive than a multi-camera setup, the single-camera better fit the design goals.

3.5 Controller Architecture

The final architecture decision that needed to be made was to identify which division of functions and method of data communication should be used. The selection affects not only the language used but also the division of computing responsibilities. There are certain unchangeable components to the system. The IRB 120 robot will run only off its internal RAPID commands. The ultrasound probe will remain an external device from which DICOM and image data can be imported. Finally, the probe tracking camera will remain a serial input regardless of internal data flow.

The most obvious consideration is to use ROS. The 'Robot Operating System' provides a stable platform for communication between separate 'nodes' implementing individual functionality. The greatest strength of a ROS-based system is the ability to incorporate 3rd party modules and the 'plug and play' nature of modules making it easier to implement and test individual components of the system. The most immediate drawback of ROS is the overhead in processing and complexity and the necessity for adding another Linux machine to run ROS. The communication between ROS and the ABB arm is achieved through a 3rd party package implemented in RAPID that converts the ABB industrial arm into a ROS node. Figure 19 contains a proposed ROS-based system layout; the majority of the processing is done on the Linux machine, taking advantage of the existing ROS nodes for processes such as April tag detections and path planning.

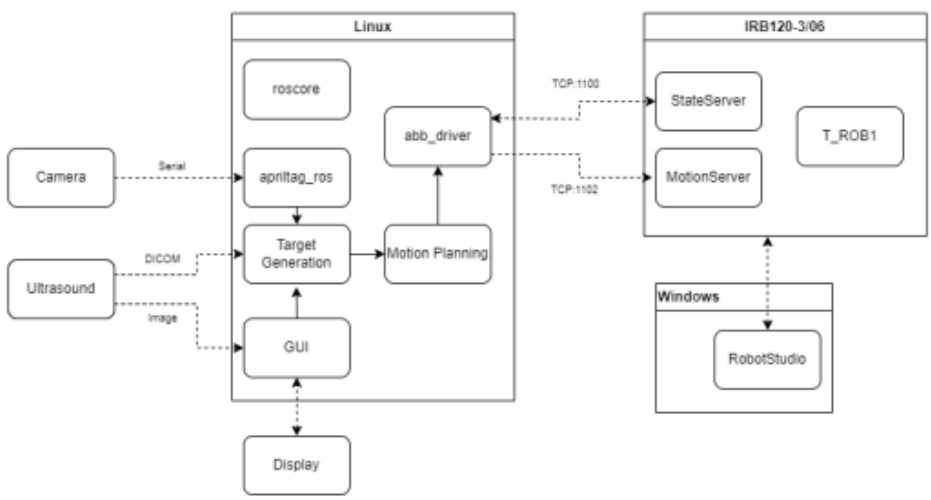

Figure 19: Diagram of ROS based system architecture

The existence of tools onboard the ABB arm for path planning and command execution in the native RAPID makes it possible to design an architecture that performs all higher-level tasks onboard the IRB120 arm, as seen in Fig 20. This system architecture uses the FK IK and path planning tools built

into the ABB programming software. Though motion planning is much easier, the RAPID language simply does not have the capacity for certain processes, such as the AprilTag fiducial detection or external input processing from systems such as an ultrasound. This limitation makes it necessary to run certain system components separately and rely on an FTP server to transfer the information in real time to the RAPID controller. If it were possible to perform all major processes within RAPID or there was greater support for importing external sensor data, implementation of a RAPID-based architecture would be appealingly simple; however, with the necessity of still implementing external processes, the limitations of working in RAPID outweigh any benefits in simplicity.

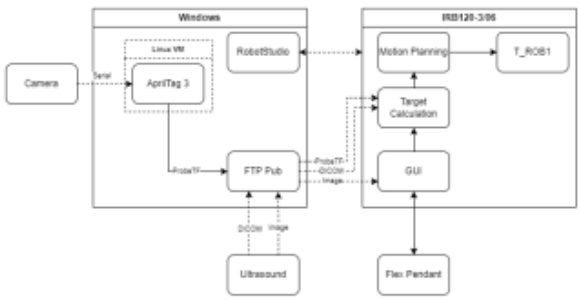

Figure 20: Diagram of RAPID based system architecture

Of the two potential architectures, I implemented this project in ROS. The primary controller for the robot will be implemented on a standalone Linux machine that is networked into the ABB arm and a Windows machine used to run the ABB programer RobotStudio.

3.6 Intended Workflow

Laying out the narrative of an ideal procedure using this system allowed me to identify several essential requirements.

The patient arrives at the physician's office for a scheduled renal biopsy. The procedure is performed in-office by a single interventional radiologist; after preparing the patient by positioning them on their stomach or side on the medical bed and applying local anesthetic, the procedure begins. Activating the robotic arm across the patient from the physician, it proceeds into a raised pose where the camera in the end effector has a clear view of the work area. The physician begins their examination with just the ultrasound probe, identifying the portion of the kidney to be biopsied and determining the best approach angle. When confident in their inspection, the physician presses a button to save a snapshot of the current ultrasound image and the probe's current position and orientation. The physician can precisely indicate the biopsy

target using the saved image and plan the needle angle within the plane. With the operation set up, the physician triggers the arm to lower. The robot orientates itself so that the required biopsy gun can be loaded and localized. The robot will then reorientate, bringing the needle into the correct orientation while remaining a safe distance from the entry site. The robot is then guided in by hand, applying a gentle corrective force to stay aligned on the planned trajectory. Suppose the physician needs to change the entry location. In that case, the positional axes can be 'unlocked' with the tool maintaining the correct orientation and the new needle trajectory displayed over the planning image. When ready to proceed with insertion, the manipulator applies a smooth counter force; the needle tip position is shown on the planning image, while the physician is free to use the live ultrasound probe for both in-plane and out-of-plane inspections. As this happens, the robot checks for deflection or increased resistance, ready to give an alert or temporarily lock out the axis depending on preference. When the needle approaches the target depth, the force feedback slowly increases until the needle stops. The physician may see that the needle needs to go deeper than they had planned, then they press a button on the manipulator, releasing the virtual clutch and allowing the insertion axis to move freely. With the appropriate location reached, the biopsy tool is held rigid when released, allowing for much easier one-handed operation of the spring trigger. Next, the physician retracts the needle along the insertion axis, the force feedback limiting the speed at first to prevent potential tearing. Finally, with the needle retracted, the physician guides the robot away from the patient before it returns to a state for convenient removal of the biopsy tool. The increased targeting accuracy, the ability to freely move the ultrasound probe while making the insertion, and the lack of the need to support and operate the biopsy tool will have significantly increased the quality of the sample gathered.

4 Manipulator Design

For ease of comprehension, I assigned names to both the end effector and overall robotic system. The initial design of the end effector was named Julie, after historical figure Julie d'Aubigny; the overall surgery system was assigned the name Abu, after the 10th century physician Albucasis, credited for the invention of diagnostic biopsy.

The majority of the mechanical design work in this project was centered around the development of an end effector for the ABB arm intended to serve as a collaborative needle guide for the surgeon. The primary degree of freedom of the end effector is the needle insertion axis. The surgeon ultimately operates the insertion axis; however, I intended for the end effector to provide haptic feedback to this DOF. The end effector design must also incorporate mounting for biopsy tools and contain the camera used for ultrasound

probe tracking.

Material selection for the Julie system was influenced by the need for rapid prototyping. The majority of the structure is built around 3-D printed components held between laser-cut wood frames. These materials do not reflect the materials that would ultimately be used in the clinical application they served in this case due to price and ease of work.

4.1 Linear Axis

The core of the Julie system is the linear insertion axis. Julie's insertion axis is constructed around a pair of 8mm rods with a 'needle carriage' riding upon them on linear bearings. (LM8UU, THK, Schaumburg, IL, USA) The ends of the rods are secured in 3D-printed blocks that are then connected to Julie's frame. The carriage and rails are shown in Figure 21. When initially designing Julie, I was concerned about the potential for misalignment of the rails, causing the carriage to bind up; however, the parts and assembly proved accurate enough to avoid this issue. Position on the insertion axis is measured by a US Digital brand linear encoder mounted to the needle carriage. The position is read from an encoder strip attached to the frame. The encoder operates at an accuracy of 200 DPI for a positional resolution of approximately 0.127mm. In addition to relative position, the encoder also provides an index pulse used in the initial calibration of the Julie system.

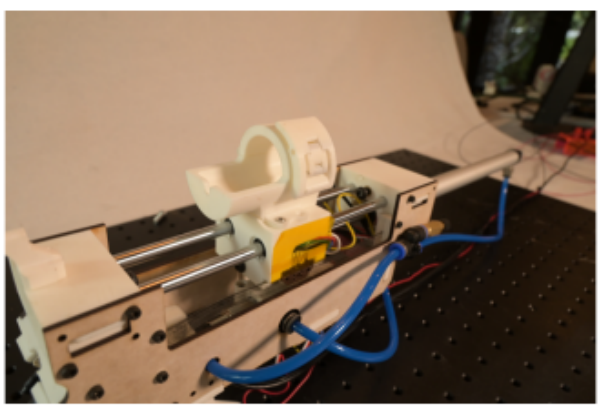

Figure 21: Image of the assembled Julie end affector focused on the needle carriage.

Post-assembly testing revealed the rod and bearing system is sensitive to foreign materials on the rails or lack of lubrication, causing excessive sliding friction. This issue is relatively minor and addressable in the context of the Julie prototype by carefully cleaning and lubricating the rails. The more concerning problem revealed in testing was that high moments on the needle carriage could result in high static friction,

increasing the risk of overshoots or jerky motion. In the ideal usage case, the operator gripping both the carriage and biopsy tool does not prove an issue; however, when installed, the biopsy tool forms a significant lever arm. Though it is not the intended mode of operation, it would be foolish of me to assume that a user would never attempt to operate the tool by gripping the end of the biopsy gun.

4.2 Haptic Feedback

The design requirements for the end factor called for force feedback along the insertion access. To achieve this, I used a pneumatic cylinder with the intention that by controlling airflow into the cylinder cell, a proportional force could be generated on the needle carriage. The initial design called for an open-loop pneumatic +system operated at Ambient pressure. However, testing revealed that an open loop implementation was too compliant. Therefore, I moved to a closed-loop system pressurized at approximately 40 psi. Two additional components are needed: a manipulator capable of modifying airflow to the cylinder and a load cell between the cylinder and carriage to measure generated force.

The load cell is installed underneath the carriage. I chose to use an s-bar loadcell (DYLY-106, Calt Sensor, Shanghai, China) to measure both positive and negative forces applied. The location of the load cell is noted in Figure 22.

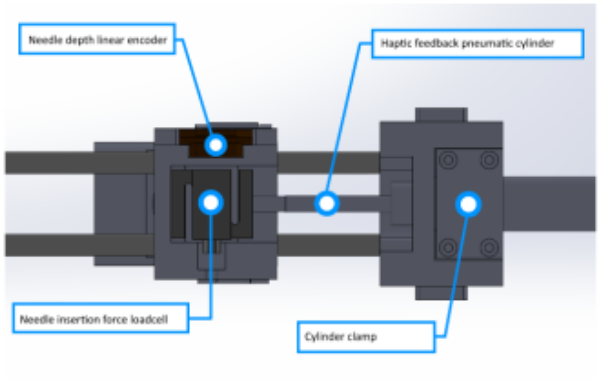

Figure 22: Labelled render of the underside of the needle carriage.

Control over the airflow presented a more interesting problem. Initially, I explored the options for solenoid actuated flow control valves; however, these proved either prohibitively expensive or excessively large in volume and weight. As a more accessible alternative, I investigated the potential of mounting a mechanically actuated valve (62005K233, McMaster-Carr, Chicago, IL, USA) to a simple 5V servo (DS3218MG, Annimos, China). Though this creates a certain latency, especially when going from binary states, it did provide a much cheaper and more accessible form of control. Initial designs made use of a valve directly

mounted to a servo; however, this proved impractical due to the requirements of range of motion of the valve itself. Eventually, I settled on the current design Figure 23, integrating a small gearbox to give a 3 to 1 reduction, extending the servo's 180° range of motion to 420°; this proved adequate for the application.

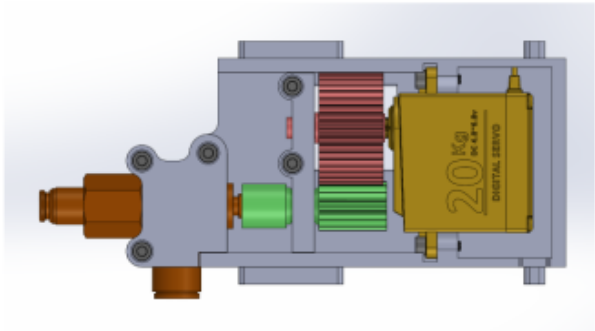

Figure 23: Render of the pneumatic cylinder flow control.

4.3 Biopsy Tool Mount

Multiple considerations informed the design of the Julie biopsy gun interface. The first and most crucial was compatibility with multiple biopsy gun systems; next was ease of operation, particularly operation by a single hand, allowing a surgeon to install and remove biopsy tools whilst maintaining a hand on the ultrasound probe. Finally, some consideration of draping requirements was necessary.

There exists a wide variety of biopsy tools used for PRBs, ideally a end effector would be compatible with most if not all potential biopsy tools. Initially I examined the commonalities between biopsy tools identifying the only totally common feature as the needle itself. Unfortunately not even the needles are consistent as different gagues are common, in addition the weight of most common biopsy guns makes suspending the tool purely by the needle non viable. Given my inability to create one design to accommodate all potential biopsy tools I instead decided the next best option would be interchangeable parts for different biopsy tools.

For the purpose of testing I acquired a Bird 14G biopsy gun as seen in Fig 1. I selected this biopsy gun as it is representitve of the most common design used and in a needle gague frequently used for PRBs. The replaceable parts i designed for the Julie system therefore are customized for this biopsy gun however they can be easily modified for alternate tools.

There are two points of contact between the Julie system and biopsy gun, the needle guide and the carriage mount. The needle guide is mounted at the front of the Julie and is responsible for the absolute positioning of the needle. The needle guide need only locate the axis of insertion and allow the needle to

slide freely within it. The second point of contact is the carriage mount, this is responsible for affixing the tool to the linear carriage. The carriage mount must allow for insertion of the tool perpendicular to the needle axis and ideally any locking or release mechanism should be operated by one hand.

The key feature of the needle guide is alignment and localization of the needle, therefore for the mounting point I settled on a T-slot design. The needle guide itself fits onto this aligning feature and consists of a simple closed ring into which the needle can be passed (Fig 24). This design is easily adaptable to different biopsy tools as a change in needle gauge merely necessitates a different bore size in the part.

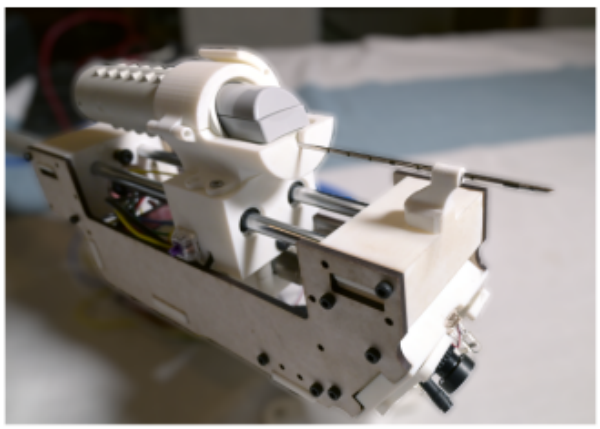

Figure 24: The Julie systems front needle guide.

The carriage mount merely holds and aligns the tool on single insertion axis, the key considerations when designing the carriage mount were ease of operation and maintaining a secure hold on the inserted tool. I chose a simple bolt pattern to mount the replaceable carriage mount due to the lack of any strict alignment requirements. To secure the cylindrical body of the Bird biopsy gun I chose a tray and cocentric over center latch as seen in Fig 25, the interior surfaces of the clamp contain alignment features to secure the tool further. The over-center clamp can be easily operated with a single hand, providing the biopsy tool can rest without shifting in the tray whilst the clamp is locked over the top; this introduces the requirement that Julie is held horizontally while loading and unloading the biopsy tool.

Draping in the context of surgical robotics refers to the requirement to keep the robotic systems behind a sanitary drape, typically lightweight plastic, unfortunately this can create some issues when it comes to interacting with surgical tools as there must be a clear boundary where the reusable robot stops, and the disposable tools begin. This is particularly complicated by any designs involving needles as having a needle penetrate through a drape compromise is the its sanitary purpose. For this reason I decided that the drape boundary for the Julie system would be underneath the replaceable components used. This introduces some issues, primarily that the components outside the drape generally have to be disposable to prevent

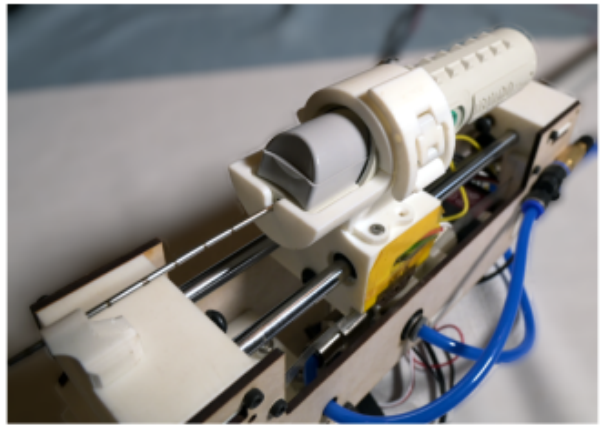

Figure 25: Over center latch used to secure the biopsy gun.

cross-contamination.

4.4 Camera Position

The final major component that needed to be integrated into the Julie system was the camera system used for locating the AprilTag fiducials while performing the ultrasound scan. The primary concern when placing the camera was the selection of hardware, packaging, and orientation. I began with the assumption that the robotic arm will reach near full vertical extension in its 'camera position'; from this I generated the approximate requirements for the camera used. I selected the Arducam B0205 package to serve as the camera. (B0205, Arducam, Kow Loon, Hong Kong) The B0205 is a preassembled USB capable camera built around the 1 / 2.7 OV2710 sensor, with an integrated lens providing 100deg FOV and a minimum focal range of 1m. This camera package provided the correct balance of high framerate, suitable resolution for the intended 40mm tag size, and FOV suitable to cover the intended work area. To achieve the maximum extension of the arm, the orientation of the end effector is limited to the near horizontal; this requirement then determines the angle the camera must be placed on the Julie device. With these restrictions in mind I selected the final angle of 55deg from Julie's horizontal plane. With the size and orientation of the camera known, I then merely had to consider packaging, a 3d printed frame suspends the camera before mounting it into a 3D printed block (Fig 26). This final placement and assembly offered the most flexibility and potential to adjust or replace the camera as needed.

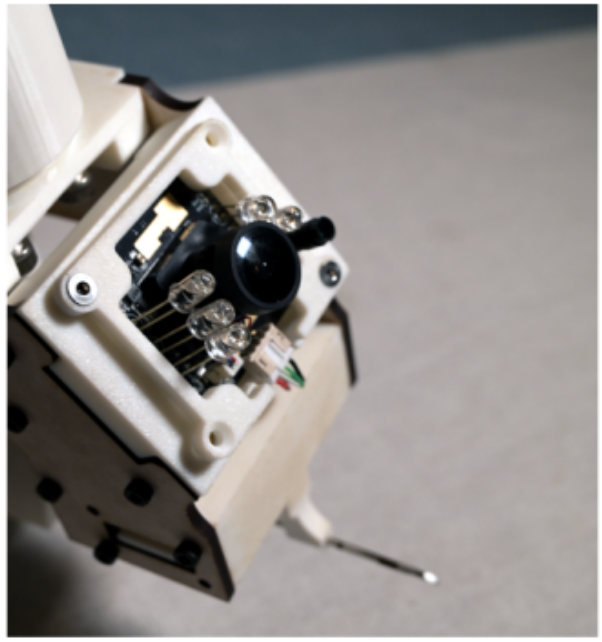

Figure 26: Camera mount on the underside of the Julie manipulator.

4.5 Electronics selection

The final design decision for the Julie end effector was the selection of electronic hardware to manage the various components. Due to familiarity with the architecture, I chose an implementation of the Arduino microcontroller. I selected the Arduino Micro for its onboard ADC, SPI interface, and ability to operate at the intended 5V. The Arduino Micro could gather the data from all the sensors in the Julie system using both custom code and some 3rd party libraries. The Abu system controller communicates via the built-in USB serial interface with the Julie board.

The choice of the Arduino Micro did present some issues, primarily the need to introduce an external power supply, as while the board has an in-built 5V regulator, it was incapable of outputting suitable current to drive all the components of the Julie system. The other significant drawback of the Arduino microcontroller is the implementation of only two interrupt pins; while the board operates at a high enough refresh rate for most of the sensors present, the linear encoder functions best when interrupt pins can be provided for both A, B, and Index signals. I was forced to compromise connecting A and index to interrupts but leaving B connected to a standard digital input; though this degrades sensor performance, I deemed the slight loss in accuracy acceptable.

The electronics were assembled on a solderless breadboard that was then mounted to the underside

of the Julie system. This placement prevented additional volume to the Julie assembly and allowed for easy cable routing around the arm mounting block. The only significant issue encountered with this choice of breadboard location was in constructing a suitable 'rolling loop' of wires between the needle carriage and breadboard, specifically in ensuring the entire bundle adequately feeds with carriage insertions and retractions. This issue was addressed mainly by the inclusion of suitable wire routing features and bundling of the loop with Kapton tape to reduce friction; however, this solution would not be acceptable in a clinical setting and, though reliable enough for my purposes still presented a significant enough failure rate that I would want to see it replaced if this design was continued.

4.6 Arduino ROS Interface

Using an Arduino required me to address the issue of managing communication between the Julie end effector and the ROS controller. While practical for onboard communication and convenient in size and compatibility, the Arduino microcontroller does not have the necessary networking capabilities for traditional ROS LAN communication. While I could have selected an Arduino microcontroller with networking capabilities such as those built around the ESP32 IC, the additional processing overhead necessary to run a ROS node would significantly increase the refresh rate and thus degrade sensor accuracy; alternatively, the selection of a larger, more powerful controller such as a Raspberry Pi 3 would have integrated both communication and enough processing power to run a ROS node, but at the cost of size and weight. As the singular purpose of the microcontroller on the Julie system was to relay sensor data and targets for the haptic feedback servo, I instead decided on a bare-bones approach using the inbuilt USB driver for serial communication.

I relied on the 3rd party ROS node rosserial and accompanying rosserial_arduino Arduino libraries to implement this communication. These libraries establish a serial communication protocol between the Arduino microcontroller and the Abu ROS controller. I start virtual ROS Publishers and Subscribers on the microcontroller, the relevant data is serialized and transmitted, and the rosserial node makes the publishers and subscribers available to the Abu ROS environment. Figure 27 contains the applicable portion of the data flow diagram covering this serial communication.

My primary concern with serial communication in this application is latency and refresh rate. Delay transmitting sensor data increases uncertainty in the robot state, whereas low refresh rates reduce precision. These concerns do not apply to full CPU ROS implementation as each publisher and subscriber are executed in individual threads; however, the single-threaded nature of Arduino code meant I had to take special care. I took several necessary measures to find an optimal balance between data accuracy and precision from the

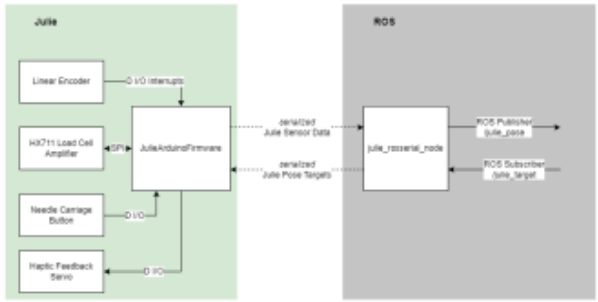

Figure 27: Rosserial data flow for communication with the Arduino microcontroller in the Julie end-effector.

Julie system.

The first and most straightforward method of optimizing for serial communication was minimizing serial message sizes. To do this, I had to reduce data sizes in the ROS msg definition to match the ranges of values sensor readings can provide. The one sensor for which I did not minimize data size was the reading of the load cell provided by the HX711 load cell amplifier, which retains a high accuracy 64bit floating point integer. I chose not to reduce the load cell reading because collecting and scaling a moving average of sensor readings at the higher baud of the HX711's SPI interface is much more efficient.

The subsequent optimization for serial communication was to minimize any onboard preprocessing or complex execution on the microcontroller. Though it would have been possible to implement higher logic, such as the state machine for the Julie end-effector onboard the microcontroller, doing so would have only increased the load on the single-threaded CPU. With the much more powerful Linux system available, I chose to minimize any processing done on the Arduino instead of implementing any requirements as a ROS node. I reduced the code on the Arduino to collecting and transmitting sensor data and outputting a PWM signal to the haptic feedback servo.

The final method I implemented to optimize the rosserial interface was to tune serial communication parameters to my specific choice of hardware. To determine optimal parameters, I experimented by publishing messages with timestamps from the Arduino microcontroller and then logging the timestamps when each message arrived in ROS. The two parameters related to rosserial communication that I can modify are the message frequency and topic queue size; other relevant parameters, such as message size and serial baud rate, are defined externally by hardware or software constraints. The topic queue length refers to the size of the FIFO queue used for the asynchronous handling of messages, I sought to minimize this while not losing crucial information. The message frequency refers to the rate at which messages are published on a topic, as the Arduino code runs and publishes continuously; this is equal to the execution time of the Arduino loop() function.

Message Frequency (Hz)	100	200	500	1000	2000
Queue Size	1	5	10	20	50

Table 7: Rosserial parameters tested

For testing, I evaluated the parameters listed in Table 7 using a baud rate of 57600 and a '/julie_pose' message modified to include a timestamp. I collected data for approximately 4 seconds. After examination of the results, I chose a message frequency of 500 Hz with a message queue size of 10. By selecting these parameters, I achieved a mean latency of approximately 2 milliseconds with no excessive latency spikes as seen in Figure 28.

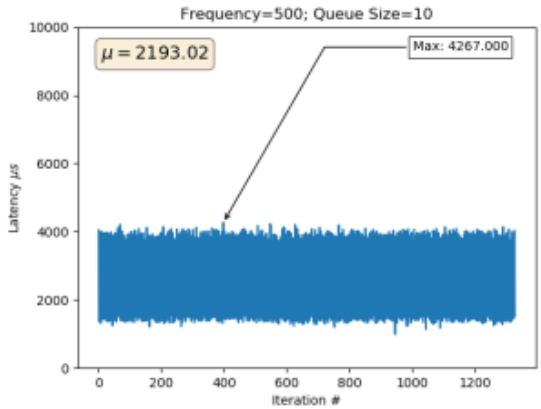

Figure 28: Plot of /julie_pose message latency.

4.7 Julie Controller

I implemented the control logic for the Julie end effector as a ROS node. The 'julie_controller is responsible for initializing and operating the Julie end effector. I designed the operation of the Julie end effector as a state machine as diagrammed in Figure 29. The julie_controller node is responsible for handling the sensor inputs, triggering sensor calibration, transitioning between end effector states, and publishing both the camera and needle tip transform once a biopsy tool is loaded. The final responsibility of the julie_controller is to manage the haptic feedback by dynamically swapping between the force and positional PD controllers.

I implemented the Julie state machine using a simple pattern reused throughout this project. By choosing the pattern detailed in Figure 30, the state machine was context-independent and easily expandable; as I stored no instance-level data within each state, I implemented the state machine with static State instances.

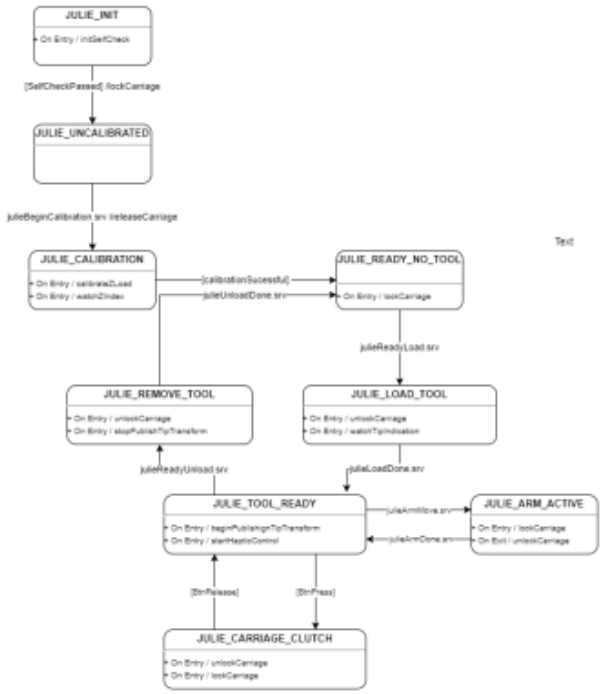

Figure 29: Diagram of state machine used to control the Julie end-effector.

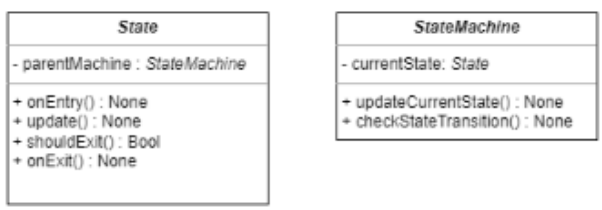

Figure 30: Diagram of the abstract state machine pattern implemented in this project.

The camera and needle tip transformations are calculated and published by the Julie control node. In addition to publishing the location of the needle tip and camera an additional 'needle tip guide' transformation is maintained for use in path planning. Figure X indicates the coordinate frames of all three transformations relative to the origin of the Julie end effector. The transformation matrices $H^{camera}_{julie\_origin}$ and $H^{guide}_{julie\_origin}$ are both static whereas $H^{needle}_{julie\_origin}$ is calculated using the insertion axis encoder value and a needle position offset measured each time a tool is inserted. EQUATIONS

A pair of PID controllers manage the Julie end effector's haptic feedback along the insertion axis. When establishing haptic feedback for needle insertion, I identified two key goals of operation: establishing constant even force when moving the needle and providing gentle restraining force to control the needle tip position when approaching the intended needle location. To implement these separate control modalities onto the same system, I used two different PID controllers that I switched between as the situation dictated.

The first PID controller is the positional control intended for use as the needle makes the final approach (¡30mm) to the biopsy sample location. The positional controller is a closed loop taking the readings from the linear encoder as an input and directly affecting the haptic servo position, affecting the restraining force applied to the needle carriage. The force control PD loop also controls the haptic servo position but it takes the net force differential measured by the load cell as its input. When implementing the force controller I made the setpoint for the experienced force differential static but configurable, based on my testing I found a force target of 35N optimal for smooth precise control but it may vary for other users. I experimented with variable force curves to apply a different force profile for insertion and extraction or to use force curves with a linear or exponential force relative to the distance to the target. I could not explore this idea as deeply as I would have liked, and non-static force curves remain of value for future examination.

When switching between the two PD loops, the most important factor is consistency for the operator. I initially experimented with making the switch between force and distance PD at a fixed distance to the biopsy target location. While it was possible to tune the handover distance to enable a smooth insertion the stability of this solution varied significantly based on carriage velocity, target force differential, and biopsy medium resistance. As an alternative, I examined making the swap when both controllers output the same control signal; this ensured smooth swapping between controllers and had the added benefit of swapping to force control on extraction much sooner. To prevent infinite swapping when the carriage is unmoving, both PD controllers outputting minimum control signals, I introduced additional conditions to control the selection of PD controllers as outlined in Figure 31. When inserting the needle the controller will not attempt to switch from force to positional control until the target_distance is less that 80mm. In regular operation, the 80mm boundary condition ensures a switch of control methods at 30mm when both controllers output signal curves intersect; alternatively, if the surgeon stops the insertion for any reason ¡80mm from the target position (assumed inside the sampled tissue) the positional control is immediately engaged when they resume motion. For needle extraction, measured as force differential being negative) the switch between positional and force control is enabled as soon as both controllers' PID values are equal; this allows a smooth transition from the steadily decreasing position control signal to the increasing force control. While testing the device, I found myself unsure if the constant force was needed for the needle extraction; while it was helpful for smooth operation, I often found myself using the clutch to release all force feedback for the extraction. Further input and feedback from actual operators are needed to determine if the force control should not simply be disabled when the device detects needle extraction.

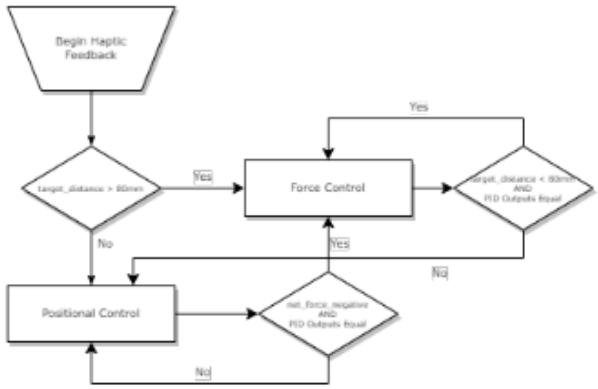

Figure 31: Logic for switching between positional and force control for the insertion axis force feedback system.

5 Abu Biopsy System Design and Programming

Once the Julie end effector had been designed and assembled, the remaining work centered around integrating the ABB robotic arm, ultrasound probe tracking, and UI to create the complete Abu system. As I had decided that the Abu system would use ROS, I implemented most of these features in Python.

The Abu systems core code runs on an Intel NUC 6i7KYK running Ubuntu 18.04.6 and ROS Melodic. I selected a post end-of-life ROS distribution for compatibility with certain required libraries. The primary driving factor behind my selection of the Intel NUC was processing capacity; the most strenuous task needed was the image processing for Ultrasound probe tracking. I selected the 2.6GHz i7 CPU for its multithreading capacity, as dedicating more threads to the AprilTag detector will increase speed while maintaining detection range.

5.1 ABB Arm Integration

To enable control of the ABB industrial arm at the core of the Abu system in ROS, I used the ROS-Industrial abb_driver package to establish TCP/IP control and communication between a ROS node and the IRC5 controller attached to the arm. The abb_driver consists of two major components ROS nodes, and servers running on the IRC5 controller. ROS nodes receive and publish the ABB arm's current state and subscribe to and transmit joint trajectory commands to the ABB arm. On the IRC5 controller, two servers implemented in ABB's native RAPID programming language connect to the TCP/IP ports to publish and receive data. I detailed the relationship and data flow between ROS and the ABB arm in Figure 32. I needed to implement minor modifications and bug fixes in the RAPID code to account for my specific hardware

configuration and firmware updates to the IRC5 controller.

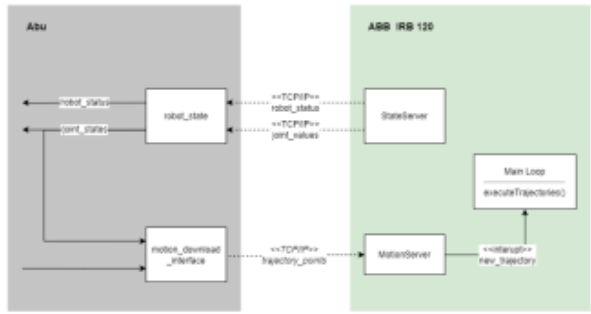

Figure 32: Data flow for abb_driver TCP/IP communication with ABB IRB120 arm.

As previously mentioned personal circumstances required me to complete this MQP remotely meaning I lost access to the physical ABB arm for testing and execution. Before beginning remote work I had connected and enabled control of the physical arm via the abb_driver so I knew that portion of the project was functional; however, I still needed a virtual implementation of the ABB system for testing. Fortunately, ABB provides a robot simulator inside their RobotStudio development suite; this simulator runs a virtual instance of the IRC5 controller while simulating the physical hardware. In prior experience with ABB industrial arms, I had found that the RobotStudio simulation was of high fidelity so I was confident it would suit my purposes. While this did introduce a slight complication as the RobotStudio software can only be run on a Windows machine the benefit compared to simulation within ROS is both in the high fidelity of the machine recreation and that by emulating the IRC5 controller itself the simulation much more accurately reflects the performance of the physical arm.

5.2 Forward Kinematics

In controlling the Abu system, it is necessary to calculate the position in 3D space from the ABB arms vector of joint angles. This transformation from the robot and world origin at T_{origin} to the end of the arm T_6 is used for ultrasound probe tracking and calculating needle tip location during insertion.

To calculate the forward kinematics of the ABB arm I used the method outlined by Denavit and Hartenberg for assigning joint frames and calculating transform matrices.[35] Figure 33 contains the joint frames I assigned for the ABB IRB120 arm in its zero position; I then took measurements of the physical characteristics of the arm to calculate the DH parameters listed in Table 8. Next I imputed the parameters into Equation 1 to calculate the transformations between each joint (Eq 5.2-5.2). These individual transformation matrices can be multiplied together to give H_0^6 (Equation 2) the transformation from robot

Joint i	$\theta_i[rad]$	$d_i[mm]$	$a_i[mm]$	$\alpha_i[rad]$
1	q_1	290	0	$-\pi/2$
2	$q_2 - \pi/2$	0	270	0
3	q_3	0	70	$-\pi/2$
4	q_4	302	0	$-\pi/2$
5	q_5	0	0	$-\pi/2$
6	q_6	72	0	0

Table 8: D-H parameters of the ABB IRB120

origin to manipulator.

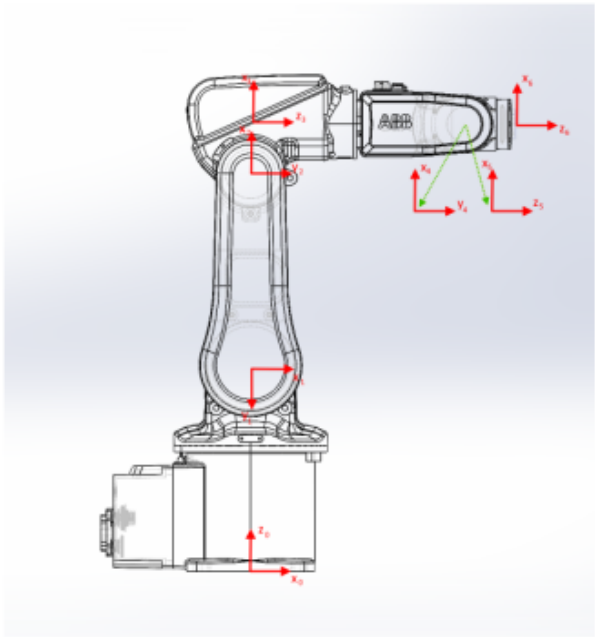

Figure 33: Diagram of frames used to define ABB IRB120 robot.

$$H_n^{n+1} = \begin{bmatrix} cos(\theta_n) & -sin(\theta_n)cos(\alpha_n) & sin(\theta_n)sin(\alpha_n) & a_n cos(\theta_n) \\ sin(\theta_n) & cos(\theta_n)cos(\alpha_n) & -cos(\theta_n)sin(\alpha_n) & a_n sin(\theta_n) \\ 0 & sin(\alpha_n) & cos(\alpha_n) & d_n \\ 0 & 0 & 0 & 1 \end{bmatrix} \tag{1}$$

$$H_0^1 = \begin{bmatrix} cos(q_1) & 0 & -sin(q_1) & 0 \\ sin(q_1) & 0 & cos(q_1) & 0 \\ 0 & -1 & 0 & 290 \\ 0 & 0 & 0 & 1 \end{bmatrix} \quad H_1^2 = \begin{bmatrix} cos(q_2 - \pi/2) & -sin(q_2 - \pi/2) & 0 & 270cos(q_2 - \pi/2) \\ sin(q_2 - \pi/2) & cos(q_2 - \pi/2) & 0 & 270sin(q_2 - \pi/2) \\ 0 & 0 & 1 & 0 \\ 0 & 0 & 0 & 1 \end{bmatrix}$$

$$H_2^3 = \begin{bmatrix} cos(q_3) & 0 & -sin(q_3) & 70cos(q_3) \\ sin(q_3) & 0 & cos(q_3) & 70sin(q_3) \\ 0 & -1 & 0 & 0 \\ 0 & 0 & 0 & 1 \end{bmatrix} \quad H_3^4 = \begin{bmatrix} cos(q_4) & 0 & -sin(q_4) & 0 \\ sin(q_4) & 0 & cos(q_4) & 0 \\ 0 & -1 & 0 & 302 \\ 0 & 0 & 0 & 1 \end{bmatrix}$$

$$H_4^5 = \begin{bmatrix} cos(q_5) & 0 & -sin(q_5) & 0 \\ sin(q_5) & 0 & cos(q_5) & 0 \\ 0 & -1 & 0 & 0 \\ 0 & 0 & 0 & 1 \end{bmatrix} \quad H_5^6 = \begin{bmatrix} cos(q_6) & -sin(q_6) & 0 & 0 \\ sin(q_6) & cos(q_6) & 0 & 0 \\ 0 & 0 & 1 & 72 \\ 0 & 0 & 0 & 1 \end{bmatrix}$$

Transfer frames for ABB IRB120 robot calculated using D-H parameters.

$$H_0^6 = H_0^1 H_1^2 H_2^3 H_3^4 H_4^5 H_5^6 \tag{2}$$

I implemented the forward kinematics into a ros node abu_fk that subscribes to /joint_states and publishes the transformations using the tf_broadcaster package. Combining the abu_fk transforms with the ones published by julie_controller allows for the continuous calculation of transforms to the camera, needle guide, and needle tip (Eq 3-5).

$$H_{origin}^{camera} = H_0^6 H_{julie\_origin}^{camera} \tag{3}$$

$$H_{origin}^{needle_guide} = H_0^6 H_{julie\_origin}^{needle\_guide} \tag{4}$$

$$H_{origin}^{needle_tip} = H_0^6 H_{julie\_origin}^{needle\_tip} \tag{5}$$

5.3 Inverse Kinematics and Path Planning

Initially outlining the required work for this project, I intended to implement inverse kinematics and path planning myself; however, restrictions of time and emerging complexity in other areas required me to use

third-party libraries for these functions through the ros 'moveit' implementation. Moveit is a comprehensive third-party tool for robotic manipulation; I made use of Moveit's integrated inverse kinematic solver and integrated path planning and trajectory generation.

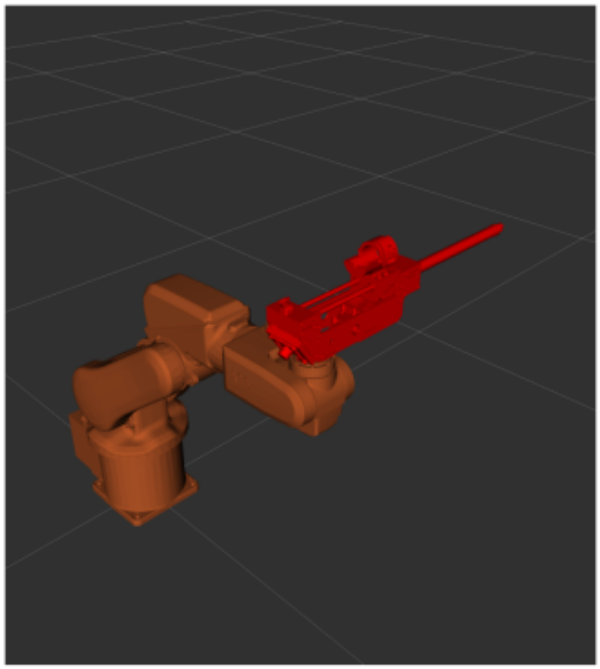

Figure 34: Abu robot in the movement planning software Moveit.

Before using Moveit, I first had to define the robotic system in URDF (Unified Robotic Design Framework). Fortunately, a URDF file for the ABB IRB 120 exists in the abb_experimental git repository. I defined the Julie end effector in URDF and then wrote a macro to attach Julie to the ABB IRB 120 arm and load both into a scene that Moveit can manipulate. (Fig 34) With just the robot model alone, I could perform IK and path planning; however, to implement obstacle avoidance, I required a model of t+6he work area. The general boundaries of the work area have already been established in Figure 11; however, the one major unknown factor is the patient's position. I used a generic 3D model to create the environment used for simulations seen in Figure 35; however, generating a scan this detailed of an actual patient is beyond the capabilities of the Abu system. Even if I generated a thorough scan of each patient, I could not use it as the patient being unsedated will likely move or be repositioned between setup and actual operation. I intend to resolve this lack of detailed work area through collaborative robotics, by putting the final positioning of the arm in the control of the surgeon they are able to approach the patient while compensating for any variation in position or body shape. Using this collaborative approach, the patient's collision geometry can be generalized to a cylindrical shape covering the patient's body and establishing the boundary of the closest

automated approach. (Fig 36) I implemented the patient boundary and geometry to establish the work area limits in URDF and integrated their import into the Abu scene macro.

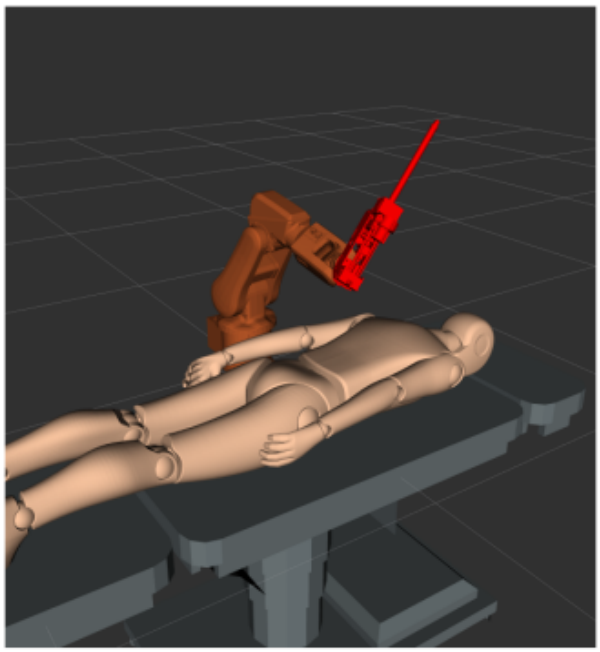

Figure 35: Abu robot with simulated work area.

With the workspace defined, I next defined the key poses for the robot so that I could calculate paths between them. Certain poses such as stowed, camera observation, and tool installation/removal are static (Fig 37); these I define relative to the robot origin. The remaining significant poses are involved in the approach to the insertion location, and I defined them relative to $T_{insertion}$, a point calculated to lie on the patient boundary with the insertion axis orientated to intersect the biopsy target. I will return to the calculation of $T_{insertion}$ in a future section; for path planning, $T_{insertion}$ can be considered an arbitrary point assumed to meet the earlier definition. Figure 36 contains the dynamic points calculated relative to $T_{insertion}$ and the robot's path between them. All of these poses are calculated and defined within the abu_path_planning node.

With the set of fixed and dynamically calculated poses, the remaining requirement is to specify the path-planning algorithm used to generate trajectories between these points. Given the relative simplicity of the workspace, the complexity of the robot, and the lack of a need for excessive traversal, I selected an implementation of Rapidly-exploring Random Trees (RRT). I considered the use of a multi-query planner such as the Probabilistic Roadmap Method (PRM), though the use of PRM would significantly reduce the runtime calculation needed; the size of the solution space that requires pre-computation must be considered. In addi-

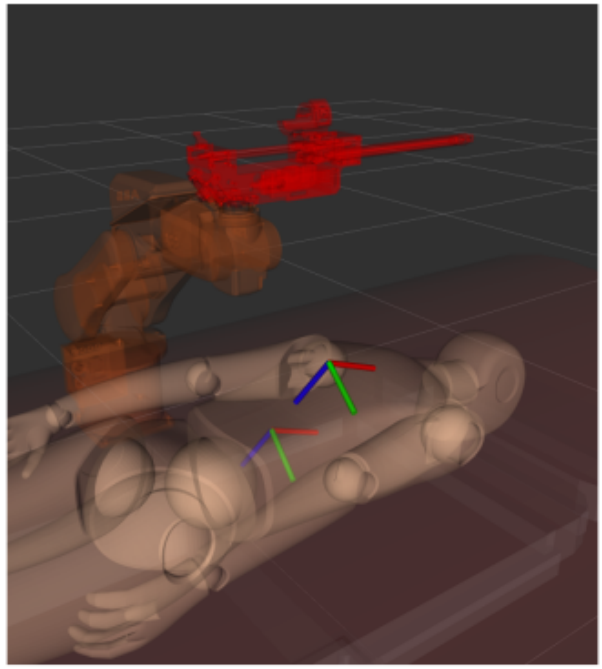

Figure 36: Abu robot with simulated work area.

tion, reliance on PRM would negatively impact the potential to expand the system with dynamic workspaces. The calculation time for the bidirectional RRT method I selected (RRTConnect) is not unreasonable for the application, and suitably smoothed the trajectories it generates are simple and effective.

After calculating the trajectory I display a preview of the planned movement to the surgeon as seen in Figure X, before executing the movement on the surgeon's confirmation. Eventually, I would prefer for the movement to be automatic; however, given the current hardware used it remains best practice to keep a human in the loop before executing any major movements.

Once the robot has executed the trajectories to the edge of the patient boundary, my preferred implementation would see the surgeon guide the robot's final approach to the patient by hand. This form of manual guidance is not possible with the robotic arm I am using for this project, so instead, I provide the surgeon with buttons on the GUI to jog the arm the remaining distance. The jogging is aligned with the z-axis along the needle insertion path and the x-axis aligned along the length of the operating table. Jogging control for this final approach is positional only as the robot maintains orientation to direct the needle at the biopsy target automatically.

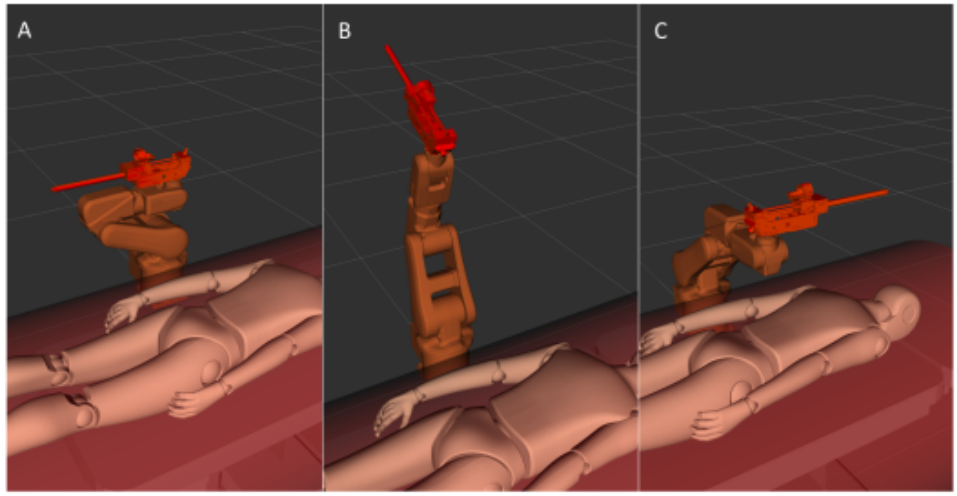

Figure 37: Static configurations of the Abu system. Pose A is the storage configuration assumed by the robot when not in use. Pose B is assumed to elevate the camera to localize the Ultrasound probe. Pose C is for loading and removing the biopsy tool.

5.4 April Tag Tracking

I chose to use a single-camera optical tracking system to localize the ultrasound probe; I selected the AprilTag fiducial and detection system to perform this task. AprilTag is a visual fiducial system developed in the University of Michigan's April Robotics lab.[36][37] The Apriltag system relies on 2D fiducial tags and a detection algorithm capable of identifying the position orientation and identity of all tags in a particular image. To use AprilTags to track the ultrasound probe, I had to design a method to attach the tags to the probes, then implement an apriltag_ros node with appropriate calibration for the camera on the Julie end effector.

I selected the tagStandard41h12 family as I had no specialist requirements, from the resolution of the Arducam B0205 I determined a 40mm size would be reliably detectable at the distance required. Once I knew which tag I would use, the next step was to determine how to attach those tags to the ultrasound probe to enable detection without significantly impacting the easy use of the transducer. A study of existing documentation on ultrasound transducer use identified a variety of grips, the most common of which are featured in Figure X. For testing, I selected a Telmed L12 ultrasound probe (L12-5L40S-3, Telmed Ultrasound, Vilnius, Lithuania) to design around as it is representative of average size and configuration for a linear or curvilinear transducer such as would be used in a PRB. While I selected a single probe to design around, my designs should remain applicable to any common transducer. The least problematic location for a fiducial flag would be to place it high and offset to one side of the transducer, selecting a height of 130mm

and offset of 50mm from the transducer origin on the L12.

Attachment to the ultrasound probe is achieved with a two piece clamshell design chosen for rigidity and adaptability to other transducers. Initially, I experimented with a two-sided vertical flag, as seen in Figure 38A; I found that while this flag design was located and tracked I ran into some issues when simulating a scan. From observation of documented procedures, I identified the need to scan at angles up to 45 deg from vertical in any direction; the fiducial tracker lost track of the vertical flagged probe as it was tilted towards the camera.

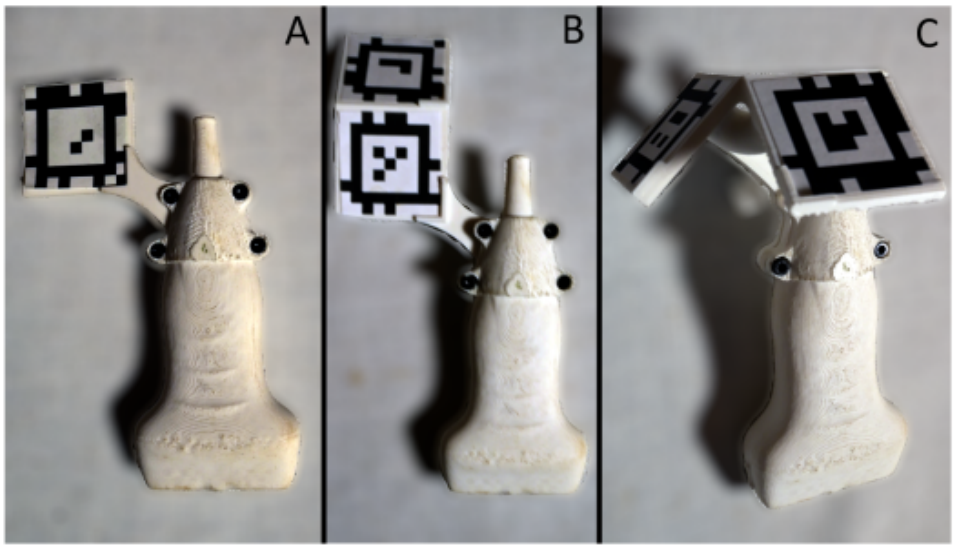

Figure 38: Different designs for attaching Apriltag flags to an ultrasound probe.

Given that a simple vertical flag could not support the full range of scanning motions, I designed and tested alternate flag configurations. The designs I assembled and tested are laid out in Figure 38. Of the designs I tried, two stood out: the single vertical flag configuration (A) and the twin angled flag (C). The vertical flagged configuration has issues maintaining tracking over the full range of angles; however, it offers simplicity and an ambidextrous design that appeals to compatibility and ease of use requirements. Alternatively, I found the twin angled flag design to be the most consistent being trackable over the full range of angles and positions at the cost of increased bulk and lack of reversibility. Neither design significantly affected my ability to grip the transducer in standard methods. Further user trials and feedback would be needed to determine which design a surgeon prefers using this system.

Once I had attached fiducials to the transducer, connecting the AprilTag detection software into ROS was relatively simple. I made each tag on the various fiducial flag designs unique and stored the transform from each to the probe origin in a lookup table. After inputting the correct parameters for

the apriltag_ros node and connecting the output of Julie's camera, the detection node began publishing transforms to each tag-detected in the live camera feed. Using the T^{tag}_{camera} transform generated by the apriltag_ros node, it is then possible to calculate the position of the transducer origin relative to the robot origin. In instances where multiple tags are detected, I chose to rely on the average of the transducer pose estimation.

5.5 Ultrasound Operation Planning

The operation of the Abu system requires the operator to plan the needle insertion point and trajectory on a 2D ultrasound image. The Abu system integrates with a commercially available ultrasound probe and provides a path-planning interface over the ultrasound image.

The industry standard for medical images is DICOM (Digital Imaging and Communication In Medicine), a file format used to store both the image data along with imaging parameters, patient info, and other data relevant to the specific imagery method.[38] Ultrasound machines can output captured images as DICOM files over a TCP/IP connection; however, DICOM ultrasound formats are designed for individual captures and thus cannot be transmitted as live images. Fortunately, the image output of the ultrasound can be accessed as a separate video stream containing the displayed image only.

The interface with the ultrasound machine is one of the areas most affected by the need to complete this project remotely; while I could print example probes for the mechanical interface I did not have access to a physical ultrasound scanner to generate actual data. To resolve this problem I relied on sample data provided by NEMA to support development around the DICOM standard (ftp://medical.nema.org). I wrote a node in ROS that simulates a Phillips 5000 series ultrasound, providing sample DICOM data in response to commands to 'capture' data.

The exact structure of the Ultrasound NEMA file is outlined in section A.6 of the DICOM standards.[39] I made use of the pydicom library[40] to extract the relevant data from the DICOM files. I extracted data from the General Image and Image Pixel sections for the ultrasound image to display for path planning. The US Region Calibration and US Image sections provided data used to calibrate and calculate the image to world transformation matrix. I did not use the patient study or series data as it held no relevance to the execution of the operation; however, this data may provide opportunities for future integration and expansion.

The surgeon makes his target selection and determines the entry trajectory on the stationary captured image. To implement this functionality, I intended to use a simple qt widget, expanding the

existing rqt_image_view plugin. A mockup of this user interface can be seen in Figure 39.

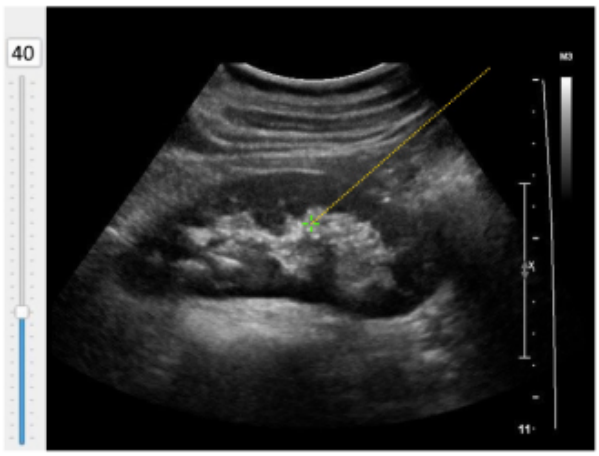

Figure 39: Mockup of the Ultrasound operation planning interface. The intended biopsy target is selected with the green cursor, and the angle of the yellow approach trajectory is set by the slider on the left.

Once I had a point in the 2D Ultrasound image selected, I then had to calculate the transform between those 2D coordinates and the 3D reference frame. Fortunately, the data needed to perform this calculation is included in the DICOM file. Figure 40 contains the coordinate systems of note when working with a DICOM ultrasound image; of particular importance is the 2D Tissue Reference, a virtual 'reference' pixel defined in the image pixel coordinate system. This reference pixel is of note to my application as for the type of US probe used during a PRB; this reference point is defined as the point of zero depth lying on the tool's centerline. I defined the probe origin reference frame to be this point exactly; therefore, the transform from the probe frame to the target frame in 3D space can be calculated from the vector from this reference pixel to the target. (Fig 41).

The vector $\hat{r}$ 6 can be calculated from r_u, r_v the points coordinates in image space, ref_u ref_v the coordinates of the reference point, and S_u S_v the scale factor of the image extracted from the DICOM in units of mm/px. I then took this calculated vector and used it to calculate H_{probe}^{target} 7 with the addition of θ the insertion angle calculated from vertical. (Fig 42)

$$\hat{r} = \begin{bmatrix} S_u(r_u - ref_u) \\ S_v(r_v - ref_v \end{bmatrix} \tag{6}$$

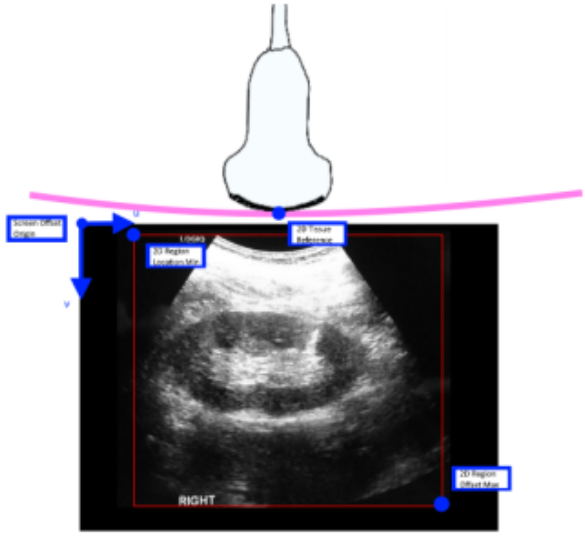

Figure 40: Diagram of key coordinates in the ultrasound image space.

$$H_{probe}^{target} = \begin{bmatrix} cos(\theta) & 0 & sin(\theta) & S_u(r_u - ref_u) \\ 0 & 1 & 0 & 0 \\ -sin(\theta) & 0 & cos(\theta) & S_v(r_v - ref_v) \\ 0 & 0 & 0 & 1 \end{bmatrix} \tag{7}$$

5.6 Abu Controller

Once I had implemented each of the individual components of the Abu syste, the only remaining task was to write an abu_control node to handle program flow and manage interactions between the systems. The abu_control node is structured around the finite state machine illustrated in Figure 43. State transitions within the control node are bounded by both internal robot conditions and external service calls.

Finally, to assist with the operation and testing of the Abu system, I wrote launch files with configurable parameters for various modes of testing and simulation.

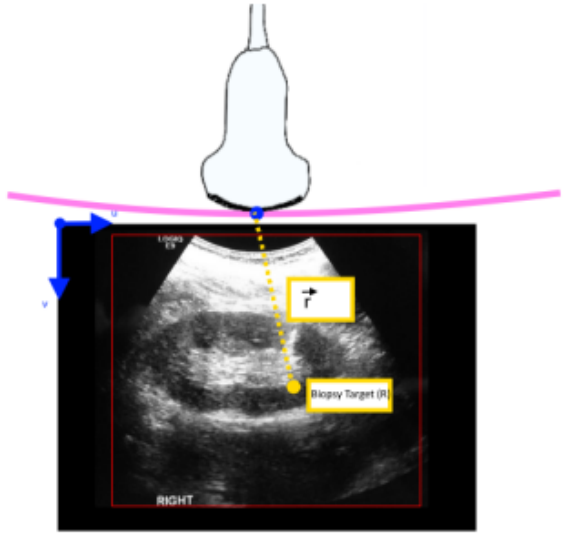

Figure 41: Diagram of the target vector calculated within the 2D image space

6 Testing

6.1 Detecting density changes in sampled tissue

When designing the Julie end effector, I included a load cell to measure the force applied to the carriage; in addition to the sensor's role in force feedback, I intended it to detect density changes in the biopsied tissue. When performing a PRB, changes in tissue density can be significant diagnostically. A drop in tissue density would indicate a fluid-filled cyst, whereas a higher density would indicate a kidney stone or a renal tumor. Though ultrasound imaging should reveal these regions of varying density, the Julie end effector's ability to detect them during insertion would give surgeons further feedback and potentially prevent mistakes.

The tissue density can be directly observed as the force resisting the needle insertion and thus is measurable by the load cell within the needle carriage. Unfortunately, the needle resistance force cannot be independently measured as the measured $\Delta F8$ is a product of F_{app}, F_{slide}, $F_{feedback}$, and F_{res}; the operators applied force, sliding friction of the assembly, force feedback applied by the cylinder, and the insertion resistance force respectively. This relationship does apply some restrictions on density detection, primarily that the detection is only possible when the carriage is moving. Additionally, the force feedback mechanism, if active, would be actively attempting to compensate for any changes in F_{res} by bringing the measured ΔF back to a set value. Though the force feedback does present some issues regarding the

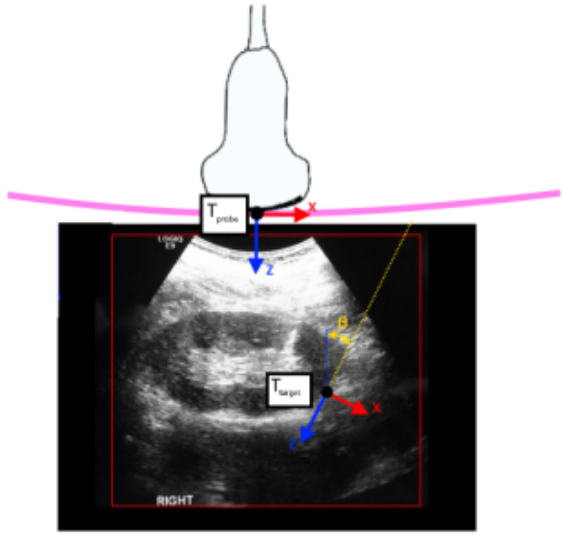

Figure 42: Relationship between probe and target coordinate frames.

collection of accurate measurements, the impulse change in measured ΔF should be detectable.

$$\Delta F = F_{app} - F_{slide} - F_{feedback} - F_{res} \tag{8}$$

I set out to test the Julie end-effector's ability to detect three significant density changes: regions of lower density, regions of high density, and tissue boundaries. Testing the force insertion required the construction of phantoms consisting of a uniform material of soft tissue density with inserted pockets of different density material. Fortunately, I discovered that there exists significant academic interest in cost-effective ultrasound phantoms for the purposes of training students in interpreting ultrasound images [41]. Once I had surveyed potential options I chose the procedure outlined in a 2012 article [42] for the construction of gelatin based phantoms with cist-like regions.

I began the process of casting the ultrasound phantoms by preparing a batch of clear gelatin at a ratio of ĩ10g gelatin powder per 1L of water. Unlike in the referenced paper, I did not mix in any Metamucil to the gelatin mix; this is because the purpose of metamucil in an ultrasound phantom is purely as a contrast material for ultrasound imaging. As I am not using any of these phantoms for imaging but only for density, the Metamucil was unnecessary. I cast the gelatin mixture in rectangular silicone molds with different procedures for each modeled density change. For testing regions of decreased density, I settled on cists formed of ultrasound gel; initially, I attempted to inject the gel into the gelatin as it set but found the process provided less optimal results. Ultimately, I settled on cutting slots into a cast gelatin phantom, almost filling them with ultrasound gel before using a fresh gelatin mixture to seal the open tops. To test

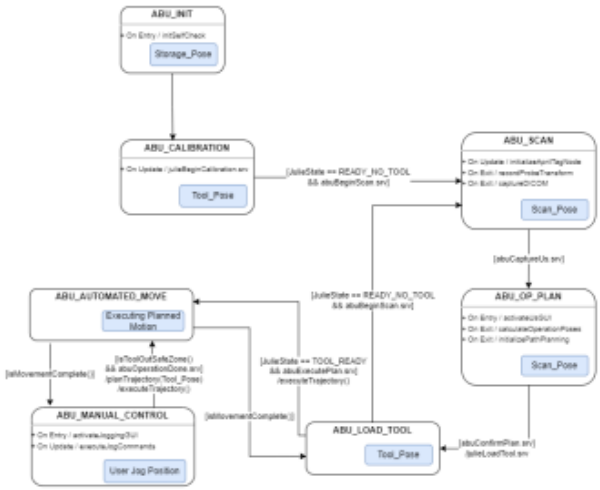

Figure 43: Diagram of the Abu systems finite state machine. Blue boxes mark the pose of the ABB arm for each state.

regions of increased density, I cast soft rubber balls into the phantom; the rubber balls were selected due to sharing a similar density to common renal tumors. Suspending the balls in the center of the phantom required a multi-stage casting process but ultimately did not prove difficult. Finally, to test boundary detection, I suspended a balloon within the gelatin phantom. The balloon within the phantom is filled with ultrasound gel; however, the test is not if the Julie system detects the lower density within the balloon but if the slight resistance of piercing the rubber skin is detectable. Figure 44 shows the casting process for the test phantoms, including the control phantom.

Figure 44: The casting process for the gelatin phantoms used for testing tissue density detection.

To perform the density measurements, the phantoms were mounted inside a raised box in line with

the fixed Julie end effector. (Fig 45) The Julie system was brought online following standard calibration procedures, with the load cell and encoder measurements logged. The biopsy needle was then inserted into the phantom by hand, applying the required force to maintain an insertion speed of $\tilde{2}0$ mm/s. For this test, I chose to disable the force feedback system; while it would be more realistic to perform this experiment with the resistive cylinder engaged, I decided that for the evaluation of the ability to detect density changes, it was beneficial to remove the closed-loop feedback from the measurements. The tests were performed in quick succession, with the biopsy needle cleaned between each insertion.

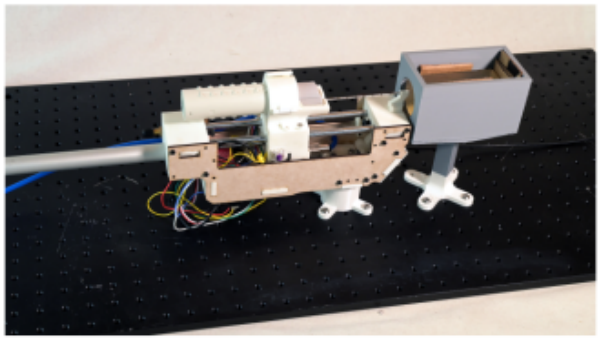

Figure 45: Julie end effector and testing jig for measuring insertion force profile.

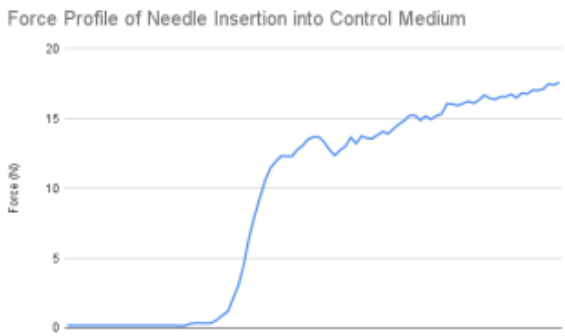

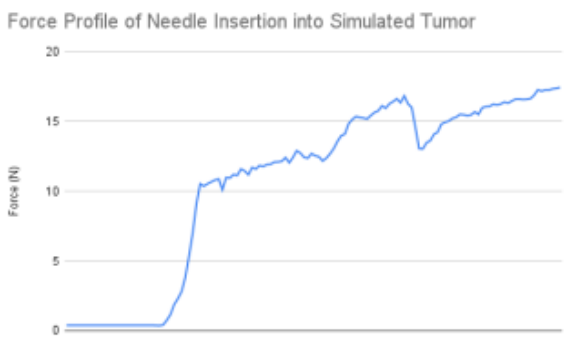

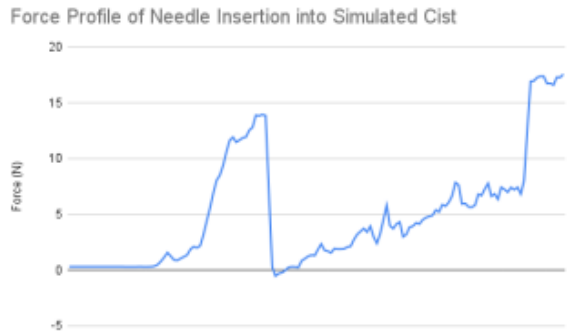

7 Discussion and Future Work

7.1 Evalutation of Full system performance

When evaluating the performance of the Abu system in general, it is tricky to balance between assessing the potential of specific ideas and systems and the practical realities imposed by the scale and scope of this MQP. The final system is far from a design that could see actual clinical use, with many small but significant changes and refinements that would need to be made before this system approaches the quality and convenience necessary for practical use. Despite this, however, in evaluating the project, I do still believe it was still successful in the evaluation of certain ideas and concepts.

The identification of lower complexity procedures, such as ultrasound-guided biopsy, as having a high potential for improved patient outcomes through collaborative robotics was correct. Beneath the certain peculiarities imposed by the prototype nature of the design, the Abu system represented a significant improvement in PRB procedure. The convenience of a robot acting as an 'assistant' by supporting and holding steady the considerably unwieldy biopsy tool is notable; however, like any assistance, I must weigh the benefits of the assistance against the inconveniences of interacting with and communicating the behavior required. It is clear that the Abu system 'jogging' keys are simply too inconvenient and unnatural to pass the threshold of convenience; however, the further development of the Abu system using a more collaborative arm would address that issue neatly. When performing the needle insertion during the biopsy, the force feedback and active depth stop features represent a significant improvement over current free-hand insertion methods.

7.2 Future Work

Considering the mechanical design of the Julie system, if I were to approach the problem again today, I would consider a different mechanical layout, potentially one that integrates a linear bearing and pneumatic cylinders machined into the body of the rails. Overall, a more compact design with less sliding friction but similar sensing capabilities would mark a significant improvement. Upgrading the valve on the haptic feedback system to be more responsive would be the next area of improvement; switching to a digitally controlled solenoid-style valve will significantly reduce the impulse response time of the positional and force feedback. Finally, an improved Julie end effector would feature additional sensing capabilities, such as needle tip detection.

If returning to this project, I would like to experiment with a more appropriate collaborative articulated arm. Replacing the ABB IRB120 with a Kuka Med or similar platform would not only be more realistic to actual surgical conditions but also allow the development and calibration of the degree of cooperation the Abu system should provide. I would like to find the balance between giving the operator complete and easy positional control of the needle and an Abu system that always gently pulls the operator's motions back toward its planned insertion point.

The area of path planning and patient detection is one where significant future developments are possible. With the current Abu system, I settled on a static oversized model of patient boundaries designed to hand off the autonomous control of the robot long before the end effector comes close to the patient. This maximum safe distance approach is driven by the inability of the robot to capture the current position of the patient in enough detail to build a model more accurately. Without adding additional sensors to the Abu system, active localization of the patient while the arm is moving may not be possible; however, I believe there are options worth exploring for developing a more accurate patient model during the 'scanning' phase. In future work, I would consider using the tracked ultrasound probe to establish a point cloud of probe 'poses' defining the boundary of the patient. Though not high resolution, a series of sweeping passes of ultrasound probe across the region of the patient's lower back could provide enough of a point cloud to infer a surface from which a more reasonable 'automation boundary' can be calculated.

7.3 Conclusions

In conclusion this project explored the design and structure of a system of collaborative robotic intervention in ultrasound guided PRB's. The final system design demonstrated the potential innovations of a robotic

'surgeon's assistant' in smaller in-office procedures. The design work around the Julie end effector focused on design for collaboration and demonstrated certain approaches to influence and data gathering from a purely 'surgeon controlled' needle insertion. The use of AprilTags as a single camera fiucial system demonstrated the potential for lower complexity and lower cost localization solutions that disconects robot assisted surgery from the infastructure requirements of more comprehenisive optical trackers. I hope that my work on this project may inform future development in this field and ultimately represents a step towards helping improve patient outcomes.

References

[1] W. Chancharoenthana, T. Kanjanabuch, W. Kittikowit, N. Srisawat, K. Tiranathanagula, K. Praditpornsilpa, K. Tungsanga, and S. Eiam-Ong, "A novel approach to ultrasound-guided percutaneous native renal biopsy: A better tissue sampling technique," *Asian Biomedicine*, vol. 8, no. 2, p. 203–210, 2014.

[2] M. Wartenberg, *Towards Hands-On Cooperative Control for Closed-Loop MRI-Guided Targeted Prostate Biopsy*. PhD thesis, Worcester Polytechnic Institute, 100 Institute Road, Worcester MA 01609-2280 USA, April 2018.

[3] S. Eslami, W. Shang, G. Li, N. Patel, G. S. Fischer, J. Tokuda, N. Hata, C. M. Tempany, and I. Iordachita, "In-bore prostate transperineal interventions with an mri-guided parallel manipulator: System development and preliminary evaluation," *The International Journal of Medical Robotics and Computer Assisted Surgery*, vol. 12, p. 199–213, Jun 2015.

[4] P. Abolmaesumi, S. Salcudean, W.-H. Zhu, M. Sirouspour, and S. DiMaio, "Image-guided control of a robot for medical ultrasound," *IEEE Transactions on Robotics and Automation*, vol. 18, p. 11–23, Feb 2002.

[5] M. Fiorentino, D. Bolignano, V. Tesar, A. Pisano, W. Van Biesen, G. D"Arrigo, G. Tripepi, L. Gesualdo, E.-E. I. W. Group, *et al.*, "Renal biopsy in 2015-from epidemiology to evidence-based indications," *American journal of nephrology*, vol. 43, no. 1, pp. 1–19, 2016.

[6] T. Hooton, R. J. Johnson, J. Feehally, and F. Juürgen, *Comprehensive clinical nephrology*. Elsevier, 2019.

[7] K. Amann and C. S. Haas, "What you should know about the work-up of a renal biopsy," *Nephrology Dialysis Transplantation*, vol. 21, no. 5, p. 1157–1161, 2006.

[8] N. J. Cozens, J. T. Murchison, P. L. Allan, and R. J. Winney, "Conventional 15 g needle technique for renal biopsy compared with ultrasound-guided spring-loaded 18 g needle biopsy," *The British Journal of Radiology*, vol. 65, p. 594–597, Jul 1992.

[9] R. N. Uppot, M. G. Harisinghani, and D. A. Gervais, "Imaging-guided percutaneous renal biopsy: Rationale and approach," *American Journal of Roentgenology*, vol. 194, p. 1443–1449, Feb 2010.

[10] I. D. Maya, P. Maddela, J. Barker, and M. Allon, "Percutaneous renal biopsy: Comparison of blind and real-time ultrasound-guided technique," *Seminars in Dialysis*, vol. 20, no. 4, p. 355–358, 2007.

[11] T. Fülöp, B. Alemu, N. R. Dossabhoy, J. H. Bain, D. E. Pruett, A. Szombathelyi, A. W. Dreisbach, and M. Tapolyai, "Safety and efficacy of percutaneous renal biopsy by physicians-in-training in an academic teaching setting," *Southern Medical Journal*, vol. 107, p. 520–525, Aug 2014.

[12] N. S. Rao and A. Chandra, "Needle guides enhance tissue adequacy and safety of ultrasound-guided renal biopsies," *Kidney Research and Clinical Practice*, vol. 37, p. 41–48, Mar 2018.

[13] S. Korbet, W. Whittier, and R. Rodby, "Changing trends in the performance of percutaneous renal biopsy from nephrologist to interventional radiologist: A single-center experience," *American Journal of Nephrology*, vol. 48, p. 326–329, Oct 2018.

[14] C. J. Nissen, V. Moreno, V. G. Davis, and P. D. Walker, "Increasing incidence of inadequate kidney biopsy samples over time: A 16-year retrospective analysis from a large national renal biopsy laboratory," *Kidney International Reports*, vol. 7, p. 251–258, Feb 2022.

[15] R. K. Gupta and R. A. Balogun, "Native renal biopsies: complications and glomerular yield between radiologists and nephrologists," *Journal of nephrology*, vol. 18, no. 5, p. 553—558, 2005.

[16] K. Sawicka, N. Hassan, C. Dumaine, A. Budd, C. Wall, T. Banerjee, H. J. Lim, P. Mondal, J. Barton, M. A. Moser, and et al., "Direction of the biopsy needle in ultrasound-guided renal biopsy impacts specimen adequacy and risk of bleeding," *Canadian Association of Radiologists Journal*, vol. 70, p. 361–366, Nov 2019.

[17] Y. Kwoh, J. Hou, E. Jonckheere, and S. Hayati, "A robot with improved absolute positioning accuracy for ct guided stereotactic brain surgery," *IEEE Transactions on Biomedical Engineering*, vol. 35, p. 153–160, Feb 1988.

[18] K. Masamune, E. Kobayashi, Y. Masutani, M. Suzuki, T. Dohi, H. Iseki, and K. Takakura, "Development of an mri-compatible needle insertion manipulator for stereotactic neurosurgery," *Computer Aided Surgery*, vol. 1, p. 242–248, Jan 1995.

[19] M. Shoham, M. Burman, E. Zehavi, L. Joskowicz, E. Batkilin, and Y. Kunicher, "Bone-mounted miniature robot for surgical procedures: Concept and clinical applications," *IEEE Transactions on Robotics and Automation*, vol. 19, no. 5, pp. 893–901, 2003.

[20] B. Davies, "A review of robotics in surgery," *Proceedings of the Institution of Mechanical Engineers, Part H: Journal of Engineering in Medicine*, vol. 214, no. 1, p. 129–140, 2000.

[21] F. J. Siepel, B. Maris, M. K. Welleweerd, V. Groenhuis, P. Fiorini, and S. Stramigioli, "Needle and biopsy robots: A review," *Current Robotics Reports*, vol. 2, no. 1, p. 73–84, 2021.

[22] "Recent fda medical device regulation and its relevance to robotics," *Tech Policy Lab*, Jan 2014.

[23] J. H. Yacoub, S. Verma, J. S. Moulton, S. Eggener, and A. Oto, "Imaging-guided prostate biopsy: Conventional and emerging techniques," *RadioGraphics*, vol. 32, no. 3, pp. 819–837, 2012. PMID: 22582361.

[24] S. Miah, P. Servian, A. Patel, C. Lovegrove, L. Skelton, T. T. Shah, D. Eldred-Evans, M. Arya, H. Tam, H. U. Ahmed, and et al., "A prospective analysis of robotic targeted mri-us fusion prostate biopsy using the centroid targeting approach," *Journal of Robotic Surgery*, vol. 14, no. 1, p. 69–74, 2019.

[25] U. Bick, R. M. Trimboli, A. Athanasiou, C. Balleyguier, P. A. Baltzer, M. Bernathova, K. Borbély, B. Brkljacic, L. A. Carbonaro, P. Clauser, and et al., "Image-guided breast biopsy and localisation: Recommendations for information to women and referring physicians by the european society of breast imaging," *Insights into Imaging*, vol. 11, no. 1, 2020.

[26] V. Groenhuis, J. Veltman, F. J. Siepel, and S. Stramigioli, "Stormram 3: A magnetic resonance imaging-compatible robotic system for breast biopsy," *IEEE Robotics & Automation Magazine*, vol. 24, no. 2, pp. 34–41, 2017.

[27] M. Chen, H. Zhao, Z. Li, Y. Zhao, Q. Tian, and T. Liu, "Development of a new needle insertion medical robot for breast tumor surgery," *2017 IEEE International Conference on Real-time Computing and Robotics (RCAR)*, Mar 2017.

[28] M. Z. Mahmoud, M. Aslam, M. Alsaadi, M. A. Fagiri, and B. Alonazi, "Evolution of robot-assisted ultrasound-guided breast biopsy systems," *Journal of Radiation Research and Applied Sciences*, vol. 11, no. 1, pp. 89–97, 2018.

[29] V. G. Mallapragada, N. Sarkar, and T. K. Podder, "Robot assisted real-time tumor manipulation for breast biopsy," *2008 IEEE International Conference on Robotics and Automation*, Apr 2008.

[30] A. Priester, S. Natarajan, and M. Culjat, "Robotic ultrasound systems in medicine," *IEEE Transactions on Ultrasonics, Ferroelectrics and Frequency Control*, vol. 60, p. 507–523, Mar 2013.

[31] Z. Jiang, S. E. Salcudean, and N. Navab, "Robotic ultrasound imaging: State-of-the-art and future perspectives," *Medical Image Analysis*, vol. 89, p. 102878, Jul 2023.

[32] S. J. Adams, B. Burbridge, H. Obaid, G. Stoneham, P. Babyn, and I. Mendez, "Telerobotic sonography for remote diagnostic imaging," *Journal of Ultrasound in Medicine*, vol. 40, p. 1287–1306, Oct 2020.

[33] D. Stoianovici, L. L. Whitcomb, J. H. Anderson, R. H. Taylor, and L. R. Kavoussi, "A modular surgical robotic system for image guided percutaneous procedures," in *Medical Image Computing and Computer-Assisted Intervention — MICCAI'98* (W. M. Wells, A. Colchester, and S. Delp, eds.), (Berlin, Heidelberg), pp. 404–410, Springer Berlin Heidelberg, 1998.

[34] F. Bruyère, J. Ayoub, and P. Arbeille, "Use of a telerobotic arm to perform ultrasound guidance during renal biopsy in transplant recipients: A preliminary study," *Journal of Endourology*, vol. 25, p. 231–234, Feb 2011.

[35] J. Denavit and R. S. Hartenberg, "A kinematic notation for lower-pair mechanisms based on matrices," *Journal of Applied Mechanics*, vol. 22, p. 215–221, Jun 1955.

[36] D. Malyuta, "Guidance, Navigation, Control and Mission Logic for Quadrotor Full-cycle Autonomy," master thesis, Jet Propulsion Laboratory, 4800 Oak Grove Drive, Pasadena, CA 91109, USA, Dec. 2017.

[37] J. Wang and E. Olson, "AprilTag 2: Efficient and robust fiducial detection," in *2016 IEEE/RSJ International Conference on Intelligent Robots and Systems (IROS)*, pp. 4193–4198, IEEE, oct 2016.

[38] C. E. Kahn, J. A. Carrino, M. J. Flynn, D. J. Peck, and S. C. Horii, "Dicom and radiology: Past, present, and future," *Journal of the American College of Radiology*, vol. 4, p. 652–657, Sep 2007.

[39] 2013.

[40] Jan 2023.

[41] J. M. Palmer, A. Little, and Q. V. Tran, "Cost-effective training models in point-of-care ultrasound for medical students in emergency medicine: An evaluation of current resources," *Cureus*, Apr 2022.

[42] M. D. Lo, S. H. Ackley, and P. Solari, "Homemade ultrasound phantom for teaching identification of superficial soft tissue abscess," *Emergency Medicine Journal*, vol. 29, p. 738–741, Sep 2011.